AIMS Energy, 9(6): 1213–1240.
DOI: 10.3934/energy.2021056
Received: 15 September 2021
Accepted: 17 November 2021
Published: 06 December 2021

http://www.aimspress.com/journal/energy

Research article

Simplified thermoelectric generator (TEG) with heatsinks modeling and simulation using Matlab and Simulink based-on dimensional analysis

Nganyang Paul Bayendang*, Mohamed Tariq Kahn and Vipin Balyan

Department of Electrical, Electronic and Computer Engineering (DEECE), Cape Peninsula University of Technology, Cape Town, WC, RSA

*** Correspondence:** Email: bayendangn@cput.ac.za; Tel: +27765404896.

Abstract: Energy sustainability is becoming paramount today with the focus being on renewable and alternative energy. This manuscript therefore embarks on clean alternative energy rooted in thermoelectricity with focus on thermoelectric generator (TEG). However, a TEG do practically needs heat-exchangers or heatsinks to properly and reliably work but heatsinks present another problem—thermal resistance, which affects a TEG power output and efficiency and thus, must be addressed. Consequently, we investigate a TEG with heatsinks model based-on dimensional analysis using Matlab and Simulink. Our research has three unique contributions. Firstly, we derived the analytical formulas for direct calculations of TEG dimensionless hot and cold sides temperature and by introducing and applying a new dimensionless parameter, the dimensionless temperature difference (DT_s). Secondly, we simplified further the new TEG dimensionless hot and cold sides temperature analytical formulas to obtain simpler and simplest forms. Thirdly, we implemented a TEG with heatsinks Matlab/Simulink theoretical model, that employs the simplified dimensional analysis, in which a TEG with heatsinks parameters of interest can be simulated to variously determine the analytical, numerical and graphical results with various optimal options to opt for, before doing a practical design.

Keywords: alternative energy; dimensional analysis; energy harvesting; TEG with heatsinks; thermoelectricity

Abbreviations and Symbols: a: TEG p-n junction thermocouple area in m^2; A_1: TEG hot side heatsink1 total surface area in m^2; A_2: TEG cold side heatsink2 total surface area in m^2; Ab: Heatsink base area in m^2; ΔT: TEG(s) temperature difference ($T_h - T_c$) in ℃ or kelvin; DT_s: TEG dimensionless

temperature difference; Eff*: TEG dimensionless conversion efficiency; h_1: TEG hot side heatsink1 convection coefficient; h_2: TEG cold side heatsink2 convection coefficient; HFD: TEG heat flux density in W/m^2; HS: Heatsinks; I: TEGs output current in ampere through the TEG; k: TEG/TEC effective thermal conductivity in W/mK; K: TEG/TEC thermal conductance in (W/K); K_1: TEG hot side heatsink1 thermal conductance; K_2: TEG cold side heatsink2 thermal conductance; L: TEG/TEC p-n junction thermocouple length in meter; LHS: Left Hand Side; n: TEG/TEC manufacturer p-n thermocouples amount used in a TEG/TEC; N: TEG number of modules required; N_h: TEG dimensionless convection conductance; N_i: TEG-HS dimensionless output current; N_k: TEG dimensionless thermal conductance; N_v: TEG-HS dimensionless output voltage (V_{os}); η: TEG thermal/electrical/conversion efficiency; η_1: TEG hot side heatsink1 fin efficiency; η_2: TEG cold side heatsink2 fin efficiency; ηhA: TEG convection conductance; $\eta_1 h_1 A_1$: TEG hot side heatsink1 convection conductance; $\eta_2 h_2 A_2$: TEG cold side heatsink2 convection conductance; ρ: TEG/TEC electrical resistivity in Ωm; ρ_e: TEG/TEC effective electrical resistivity in Ωm; P_n: TEG normalized output power; P_o: TEG output power in watt, is the difference between Q_h and Q_c; P_{os}: TEG dimensionless output power, is the difference between Q_h*(Q_{s1}) and Q_c*(Q_{s2}); Q_c: TEG heat emitted on its cold side in watt; Q_h: TEG heat absorbed on its hot side in watt; Q_{s1}: TEG hot side dimensionless heat absorbed (Q_h*); Q_{s2}: TEG cold side dimensionless heat released (Q_c*); r: TEG/TEC thermocouples p-n junction unit resistance in ohm; RHS: Right Hand Side; R_L: TEG electrical load resistance in Ω connected to the TEG output; R_t: TEG/TEC module internal resistance in ohm—also denoted as R_R in Figure 2; R_r: TEG dimensionless internal electrical resistance—also denoted as rr in Figure 2; S: TE device Seebeck coefficient in V/K; S_e: TEG/TEC effective Seebeck coefficient in V/K; $\overline{T}$: TE device average temperature ($T_h + T_c$)/2 in K or ℃; T_1: TEG hot side temperature (T_h); T_2: TEG cold side temperature (T_c); TE: Thermoelectric; TEC: Thermoelectric cooler; TEG: Thermoelectric generator; T_i: TEG hetasinks fluid dimensionless temperatures (Tis); T_{i1}: TEG hot side heatsink1 fluid dimensionless temperature; T_{i2}: TEG cold side heatsink2 fluid dimensionless temperature; T_{s1}: TEG hot side dimensionless temperature; T_{s2}: TEG cold side dimensionless temperature; T_c: Temperature on TEG/TEC cold side in ℃; T_h: Temperature on TEG/TEC hot side in ℃; T_p: TEG/TEC modules quantity in parallel; T_s: TEG/TEC modules quantity in series; V_o: TEG module output voltage in volt; V_{oc}: TEG ideal or open circuit output voltage (consider it as EMF = electromotive force) in volt; V_{os}: TEG dimensionless output voltage (N_v); V_n: TEG normalized output voltage; Z: TE device figure of merit in per K; Z_e: TEG/TEC effective figure of merit in per K; $Z\overline{T}$: TE device average dimensionless figure of merit; ZT_{i2}: TEG dimensionless figure of merit at temperature T_{i2}; ZTA: TEG dimensionless figure of merit at temperature TA ($\overline{T}$)

1. Introduction

Indicated in [1], South Africa has pledged its commitments to become a carbon reduced and green economic system, by considering a mixture of energy sources to secure energy sustainability. Upon ratifying the Paris agreement on climate change, renewable energy and energy efficiency frameworks as well as the regulatory policies have been developed and continuously fine-tuned taking into cognizance the current energy dynamics. In this regard, there is necessity and increasing demand for renewable energy to supplement and stabilize the unstable national grid, as well as for private use. These circumstances, warrant our research for an alternative energy rooted in thermoelectricity, with focus on basic residential energy sources and energy efficient loads. Basically, TEGs convert heat to DC power, whereas their dual thermoelectric coolers (TECs), reversibly converts DC power to cold and heat depending on the applied voltage polarity. If TEGs and TECs are properly designed, both can

be relatively energy efficient and helpful for essential domestic energy use such as low-voltage DC power, lighting, heating and cooling. Theoretical frameworks and applications of both TEG and TEC were comprehensively presented in [2–5]; however, they fell short of some practical aspects—which this article seeks to advance as articulated next.

In [4–9], thermoelectricity or thermoelectric (TE) devices (TEGs and TECs), require heatsinks or heat-exchangers to physically and reliably function and maintain a working temperature difference on the TEG and TEC hot and cold sides and most significantly to discharge the internal heat resulting from Joule (Ohmic) heating cause by the current flowing through the TEG/TEC. This Ohmic heating is irreversible and will become excessive if not properly managed and consequently, will cause drop in the output/cooling powers and inefficiency (change in entropy-heat flow will change direction due to increase in the cold side junction temperature). This can as well damage the TEG and TEC as a result of over-heating exceeding the hot and cold sides maximum temperature limit—which will melt the thermoelectric devices p-n junction thermocouples solder joints. The inclusion of heatsinks as a solution to alleviate this over-heating practical limitations in thermoelectric devices, unfortunately as well add/increase the TEGs and TECs hot and cold sides thermal resistances, which then oppose the ideal heat flow, hence making the TE devices inefficient.

To circumvent this thermal resistance problem resulting from adding heatsinks/heat-exchangers, various approaches have been investigated and some are stated briefly as follows. Simplified in [6] is a dimensional analysis by converting thermal resistance to convection conductance when using TEC with heatsinks—which was researched originally in [7]; however, the presentation lacks key analytical formulas. In [8], a TEG with heatsink for waste energy harvesting was analysed and optimised as a Thevenin equivalent circuit and investigated in [9] is a dimensionless model of a TEC functioning at real heat transfer state. Examined in [10], a multi-physics simulations were conducted to examine the thermal and electrical performances of a TEG module sand-witched between hot and cold blocks, whereas in [11], a parametric thermal analysis of TEG performance was done using dimensional analysis and presented in [12] is a numerical simulation and performance analysis of a TEC based-on the lattice Boltzmann method. Studied in [13] is a multi-parameters analysis and optimization of a typical TEC using dimensional analysis. Proposed in [14] is a thermal resistance matching for TEC systems whereas examined in [15], is an optimal design of a multi-couple TEG, meanwhile [16] employed a graphical approach to design TEC systems. Demonstrated in [17] is an electron-transparent TEC using nano-particles and condensation thermometry and investigated in [18] is an optimal heat-exchanger in different automobile exhaust temperatures for TEG system using dimensional analysis. From the reviewed studies, the dimensional analysis technique, especially the unique and practical approach presented in [7] to improve TE devices efficiency when used with heatsinks, is of interest. This paper with keen focus on TEG as exemplified in Figure 1, further develops the dimensional analysis, by now employing a simplified Matlab implementation to derive novel analytical formulas to directly calculate a TEG hot and cold sides dimensionless temperature.

Our study was structured around the following points. We begin with the TEG with heatsinks applicable maths developed from [6,7] with now emphasis on the new additional analytical formulas. We derived the TEG hot and cold sides dimensionless temperature, as well as the further optimal simplifications contributed relative to the shortcomings of the formulas/approach used in [7]. In a next step, we depict the TEG with heatsinks simulator easy user interface modeled with Matlab/Simulink. The presentation of our results is followed by discussions as well as validations and lastly we conclude our study with a summary.

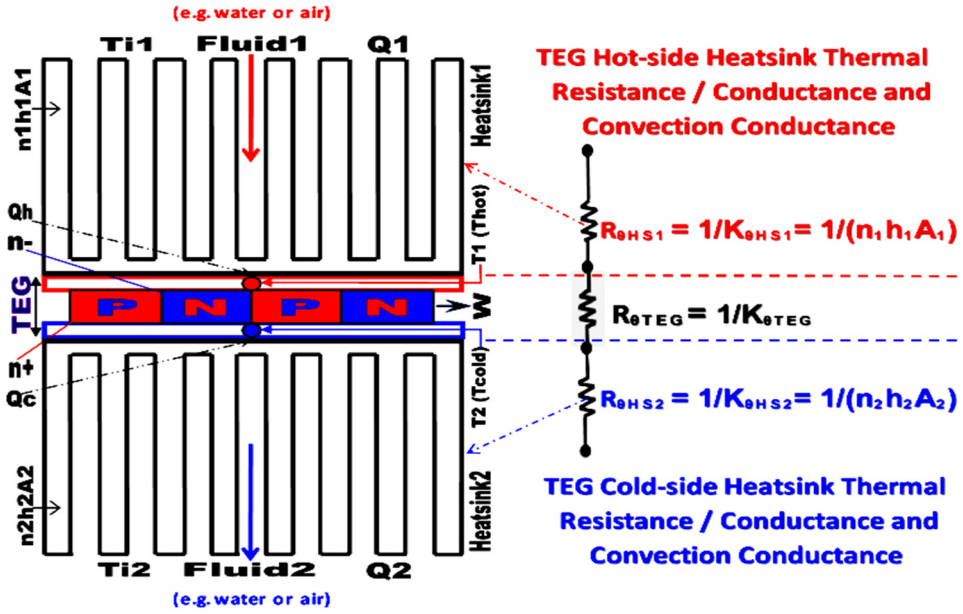

Figure 1. TEG with heatsinks on its hot and cold sides.

2. Dimensional analysis mathematics

The relevant mathematics for a TEG with heatsinks is expressed herein and we then introduce the new dimensionless temperature difference (DTs)—which is employed to simplify the apt approach given by [7]. Dimensional analysis is a technique that enables parameters with the same unit to be normalized within a minimum and maximum value, thus making them dimensionless and easier to work with, without worrying about their dimensions or unit of measurement. Nonetheless, novel in [7] is the conversion of TEG heatsinks thermal resistance to their convection conductance. This optimization technique gets rid of the TEG heatsinks thermal resistance which are harder to work with, in favour of the TEG heatsinks fluid convection conductance which are related to the TEG heatsinks fluid temperature and physically simpler to work with. This approach is pragmatic and the mathematical analysis is articulated in what follows.

TEG with heatsinks general heat flow equations:

Herein, the TEG heat flow equations, the heatsinks thermal resistance, their corresponding thermal conductance and convection conductance relationships developed from [6] are constituted as follows:

$$Q_1 = K_1(T_{i1} - T_1) \quad (W) \tag{1}$$

$$Q_2 = K_2(T_2 - T_{i2}) \quad (W) \tag{2}$$

With Q_1 and Q_2 being respectively the heat flow rates on the TEG heatsinks hot and cold sides, K_1 and K_2 are respectively the TEG hot and cold sides heatsinks thermal conductance, T_{i1} and T_{i2} are respectively the temperatures of the heatsinks fluid on the TEG hot and cold sides and lastly T_1 and T_2 are respectively the TEG hot and cold sides p-n junction temperatures. It is worthy of note that thermal resistance is the reciprocal of thermal conductance K—which corresponds to the convection conductance (ηhA) and thus, Eqs 1 and 2 in respect of the convection conductance, can be re-written as:

$$Q_1 = \eta_1 h_1 A_1 (T_{i1} - T_1) \quad (W) \tag{3}$$

$$Q_2 = \eta_2 h_2 A_2 (T_2 - T_{i2}) \quad (W) \tag{4}$$

With η_1 being the fin efficiency of heatsink1 (on the TEG hot-side), h_1 is the convection coefficient of heatsink1 and A_1 is the total surface area of heatsink1. Similarly, η_2 is the fin efficiency of heatsink2 (on the TEG cold-side), h_2 is the convection coefficient of heatsink2 and lastly A_2 is the total surface area of heatsink2.

The TEG standard ideal heat flow equations are defined as:

$$Q_h = n[(SIT_1) + (K\Delta T)] - 0.5I^2R \quad (W) \tag{5}$$

$$Q_c = n[(SIT_2) + (K\Delta T)] + 0.5I^2R \quad (W) \tag{6}$$

where Q_h is the heat absorbed on the TEG hot side, n is the number of p-n junction thermocouples used in the TEG, S being the Seebeck coefficient, I being the output current from the TEG, K is the thermal conductance (computed as ak/L, with a being the area of the TEG p-n junction thermocouple, k is the TEG thermocouple p-n junction thermal conductivity and L is the TEG thermocouple p-n junction length). $\Delta T = T_1 - T_2$ is the temperature difference between the TEG hot and cold sides, $R = nr$ is the TEG module resistance, with r being the resistance of the TEG thermocouple p-n junction and Q_c is the heat released on the TEG cold side. The three terms on the right side of Eqs 5 and 6 are the Seebeck, Fourier and Ohmic terms respectively; with S, K and R considered as temperature invariant. Now, taking into account the energy balance of the TEG with heatsinks system, Eqs 1, 3 and 5 are respectively equivalent now to Eqs 2, 4 and 6—which boils down to (with parameters T_1, T_2 and I being the unknowns):

$$Q_1 = Q_h = K_1(T_{i1} - T_1) = \eta_1 h_1 A_1 (T_{i1} - T_1) = n[(SIT_1) + (K\Delta T)] - 0.5I^2R \quad (W) \tag{7}$$

$$Q_2 = Q_c = K_2(T_2 - T_{i2}) = \eta_2 h_2 A_2 (T_2 - T_{i2}) = n[(SIT_2) + (K\Delta T)] + 0.5I^2R \quad (W) \tag{8}$$

With recognition to [7], TEG with heatsinks (HS) is optimised by defining the dimensionless parameters with regards to fluid 2 (water or air on the TEG cold side of heatsink2) and because the optimization is rendered dimensionless relative to fluid 2, fluid 2 temperature (T_{i2}) and convection conductance must be given initially. The following dimensionless maths is developed further from [6,7] as:

TEG-HS dimensionless thermal conductance (N_k):

This is the ratio of the thermal conductance K and the convection conductance ηhA in fluid 2, deduced as:

$$N_k = K/\eta hA = (ak/l)/\eta_2 h_2 A_2 \tag{9}$$

TEG-HS dimensionless convection (N_h):

This is the ratio of fluid 1 and fluid 2 convection conductances, denoted as:

$$N_h = \eta_1 h_1 A_1/\eta_2 h_2 A_2 \tag{10}$$

TEG-HS dimensionless current (N_i):

$$N_i = SI/K = SI/(ak/l) = ZT_{i2}\,(T_{s1} - T_{s2})/(R_r + 1) \tag{11}$$

TEG dimensionless temperatures (T_{s1}, T_{s2}, T_i and DT_s):

TEG dimensionless temperatures are presented as:

T_1 dimensionless temperature: $T_{s1} = T_1/T_{i2}$ (12)

T_2 dimensionless temperature: $T_{s2} = T_2/T_{i2}$ (13)

Fluids dimensionless temperature: T_i (T_{is}) = T_{i1}/T_{i2} (14)

Dimensionless temperature difference $DT_s = T_{s1} - T_{s2} = \Delta T/T_{i2}$ (15)

TEG-HS dimensionless heat absorbed (Q_{s1}):

$$Q_{s1} = Q_1/\Pi_2 h_2 A_2 T_{i2} \quad (16)$$

TEG-HS dimensionless heat released (Q_{s2}):

$$Q_{s2} = Q_2/\Pi_2 h_2 A_2 T_{i2} \quad (17)$$

TEG dimensionless output power (P_{out*} or P_{os}):

$$P_{out*} = P_{out}/\Pi_2 h_2 A_2 T_{i2} \quad (18)$$

$$P_{os} = P_{out*} = Q_{s1} - Q_{s2} \quad (19)$$

where P_{out} is the TEG output power (power delivered to the electrical load)

TEG dimensionless output voltage (V_{os} or N_v):

$$N_v = V/nST_{i2} \quad (20)$$

$$N_v = V_{os} = P_{os}/N_i N_k \quad (21)$$

TEG dimensionless conversion efficiency (E_{ff}^*):

$$Eff^* = P_{os}/Q_{s1} \quad (22)$$

NB: TEG conversion efficiency by default is dimensionless. The mentioned of dimensionless in front conversion efficiency is just for emphasis on the dimensionless analysis technique used.

TEG-HS dimensionless heat absorbed (Q_{s1}) in terms of T_{s1}:

$$Q_{s1} = N_h (T_i - T_{s1}) \quad (23)$$

TEG-HS dimensionless heat released (Q_{s2}) in terms of T_{s2}:

$$Q_{s2} = T_{s2} - 1 \quad (24)$$

TEG-HS dimensionless internal electrical resistance (R_r):

$$R_r = R_L/R_t \quad (25)$$

where R_L is the electrical load connected to the TEG output and R_t is the TEG module internal electrical resistance. NB: R_r is denoted as *rr* in the TEG-HS simulator in Figure 2.

As per [7], using the dimensionless Eqs 9–14, Eqs 3–6 reduce to the following two expressions (26) and (27) having five unknowns that must be found for T_{s1} and T_{s2} in terms of five independent dimensionless parameters of ZT_{i2} (dimensionless figure of merit at T_{i2}), T_i, N_h, N_k and R_r.

$$N_h(T_i - T_{s1})/N_k = ((ZT_{i2}(T_{s1} - T_{s2})T_{s1})/(R_r + 1)) - (((ZT_{i2}(T_{s1} - T_{s2})^2))/(2(R_r + 1)^2)) + (T_{s1} - T_{s2}) \quad (26)$$

$$(T_{s2} - 1)/N_k = ((ZT_{i2}(T_{s1} - T_{s2})T_{s2})/(R_r + 1)) + (((ZT_{i2}(T_{s1} - T_{s2})^2))/(2(R_r + 1)^2)) + (T_{s1} - T_{s2}) \quad (27)$$

As noticeable, Eqs 26 and 27 are cumbersome and unsolved further in [7] in terms of T_{s1} and T_{s2}; therefore, there are no exact analytical equations to directly compute T_{s1} and T_{s2}. Eqs 26 and 27 are awkward closed-form expressions of T_{s1} and T_{s2}, which can only be solved by using numerical analysis; as a result, a numerical method using iterations, tables, graphs and approximations were employed by [7], as well as using a computer programme (NEDO) was further recommended. Consequently, because Eqs 26 and 27 could not be simplified further by [7], T_{s1} and T_{s2} could only be expressed as in Eqs 28 and 29 as functions of ZT_{i2}, T_i, N_h, N_k and R_r for solving numerically.

$$T_{s1} = f(ZT_{i2}, T_i, N_h, N_k, R_r) \quad (28)$$

$$T_{s2} = f(ZT_{i2}, T_i, N_h, N_k, R_r) \quad (29)$$

This entire numerical process is tedious to determine T_{s1} and T_{s2}; thus, this limitation motivated our study to seek for a direct analytical and better solution(s) which are asserted next.

We now introduce Eq 15—the dimensionless temperature difference DT_s, which is used to replace $T_{s1} - T_{s2}$ in Eqs 26 and 27 to give Eqs 30 and 31 as:

$$N_h(T_i - T_{s1})/N_k = ((ZT_{i2}(DT_s)T_{s1})/(R_r + 1)) - (((ZT_{i2}(DT_s)^2))/(2(R_r + 1)^2)) + (DT_s) \quad (30)$$

$$(T_{s2} - 1)/N_k = ((ZT_{i2}(DT_s)T_{s2})/(R_r + 1)) + (((ZT_{i2}(DT_s)^2))/(2(R_r + 1)^2)) + (DT_s) \quad (31)$$

As instantly apparent, Eqs 30 and 31 can respectively and directly be solved for T_{s1} and T_{s2} independently in terms of the five dimensionless parameters ZT_{i2}, T_i, N_h, N_k and R_r. Now, making T_{s1} and T_{s2} subjects of their respective Eqs 30 and 31, we derived new analytical equations for T_{s1} and T_{s2} as given in Eqs 32 and 33 as:

$$T_{s1} = (N_kZT_{i2}DT_s^2 - 2N_kDT_sR_r^2 - 4N_kDT_sR_r - 2N_kDT_s + 2N_hT_iR_r^2 + 4N_hT_iR_r + 2N_hT_i)/$$
$$(2(R_r + 1)(N_h + N_hR_r + DT_sZT_{i2}N_k)) \quad (32)$$

$$T_{s2} = (N_kZT_{i2}DT_s^2 + 2N_kDT_sR_r^2 + 4N_kDT_sR_r + 2N_kDT_s + 2R_r^2 + 4R_r + 2)/$$
$$(2(R_r + 1)(R_r - DT_sN_kZT_{i2} + 1)) \quad (33)$$

Furthermore, by adding Eqs 26 and 27 or Eqs 30 and 31; we can easily get rid of the nonlinear quadratic terms as shown in Eqs 34 and 35 and by re-arranging and solving for T_{s1} and T_{s2}, we can further derive a simpler T_{s1} and T_{s2} novel analytical formula as shown in Eqs 36 and 37.

$$N_h(T_i - T_{s1})/N_k + (T_{s2} - 1)/N_k = (ZT_{i2}DT_sT_{s1})/(R_r + 1) + (ZT_{i2}DT_sT_{s2})/(R_r + 1) + DT_s + DT_s \quad (34)$$

$$N_h(T_i - T_{s1})/N_k - ((ZT_{i2}DT_sT_{s1})/(R_r + 1)) - DT_s = ((ZT_{i2}DT_sT_{s2})/(R_r + 1)) + (T_{s2} - 1)/N_k + DT_s \quad (35)$$

Equation (34) was re-arranged to give Eq 35, such that the left hand side (LHS) of Eq (35) constitutes T_{s1} without T_{s2} and the right hand side (RHS) of Eq 35 constitutes T_{s2} without T_{s1}. Finally, the LHS and RHS were both solved independently by equating each to zero, to easily obtain T_{s1} in terms of ZT_{i2}, T_i, N_h, N_k, R_r and DT_s (NB: now six unknown parameters) and similarly to obtain T_{s2} in terms of ZT_{i2}, N_k, R_r and DT_s (NB: now four unknown parameters) to respectively give Eqs 36 and 37 expressed as:

$$T_{s1} = (N_hT_i - DT_sN_k)(R_r + 1)/(N_h + N_hR_r + DT_sN_kZT_{i2}) \quad (36)$$

$$T_{s2} = (DT_sN_k + 1)(R_r + 1)/(R_r - DT_sN_kZT_{i2} + 1) \quad (37)$$

As seen, T_i and N_h are absent in Eqs 33 and 37, meaning these two dimensionless parameters, don't directly affects T_{s2} or affects T_{s2} indirectly through T_{s1} and DT_s; thus, making these equations insightful.

Finally, we furthermore obtained the simplest optimal analytical relationship to calculate T_{s1} and T_{s2} by utilizing a set of optimal numerical values given in [7] as: $ZT_{i2} = 1$, $T_i = 2.6$, $N_h = 1$, $N_k = 0.3$, $R_r = 1.7$ and $DT_s = 0.8$ and by substituting these values in Eq 35 and solving further, we obtain Eqs 38 and 39 as:

$$T_{s1} = 41T_{s2}/49 + (36/35) \quad (38)$$

$$T_{s2} = 49(T_{s1} - (36/35))/41 \quad (39)$$

It should be noted that, the $ZT_{i2} = 1$, $T_i = 2.6$, $N_h = 1$, at $N_k = 0.3$, $R_r = 1.7$ and now $DT_s = 0.8$ optimal values set are not arbitrarily chosen but specifically deduced optimal values, that are inter-linked to each other and obtained under the same specified operating conditions. Furthermore, parameters ZT_{i2}, T_i and N_h are initially provided or can be calculated from a chosen TEG-HS operating parameters and finally the optimal combinations of N_k, R_r and now DT_s, can all be established from the above specified dimensionless equations. NB: other optimal values set can be used in Eq 35 to get new Eqs 38 and 39 also.

Now, to validate our new T_{s1} and T_{s2} formulas, we substitute this the same chosen set of optimal values (given in [7]) of $ZT_{i2} = 1$, $T_i = 2.6$, $N_h = 1$, $N_k = 0.3$, $R_r = 1.7$ and $DT_s = 0.8$ to finally determine, compare and verify the T_{s1} and T_{s2} values by using our newly derived simple, simpler and simplest analytical formulas; respectively using Eqs 32 and 33, Eqs 36 and 37 and Eqs 38 and 39 as follows:

Using the now simple formulas (Eqs 32 and 33), T_{s1} and T_{s2} are optimally directly computed as:

$$T_{s1} = 2.1794$$

$$T_{s2} = 1.3754$$

Using the now simpler formulas (Eqs 36 and 37), T_{s1} and T_{s2} are optimally directly deduced as:

$$T_{s1} = 2.1673$$

$$T_{s2} = 1.3610$$

As seen, both these new simple and simpler optimal solutions are approximately the same. We can then also easily verify both with Eqs 38 and 39 to get the simplest solution, by substituting T_{s2} to calculate T_{s1} or vice versa. We've now introduced three new analytical sets of formulas to easily compute T_{s1} and T_{s2} without going through the cumbersome numerical process. With T_{s1} and T_{s2} easily deduced, the other dimensionless parameters and ultimately all their physical dimensional parameters, can then be worked out using Eqs 1–25.

3. Model simulator

The relevant TEG with heatsinks mathematics based on dimensional analysis was articulated in Section 2 and the formulas for T_{s1} and T_{s2} were developed and expressed analytically in respect of

the now six independent parameters ZT_{i2}, T_i, N_k, N_h, R_r and DT_s. Furthermore, T_{s1} and T_{s2} were optimally simplified and validated in terms of T_{s1} and T_{s2} using Eqs 38 and 39. As apparent, the entire numerical as well as analytical procedures could be very tedious and as well subject to errors if manually done. In view of this, a Matlab and Simulink TEG model with heatsinks on both the TEG hot and cold sides, was then implemented using the formulas asserted in Section 2. Enclosed in the simulated TEG with heatsinks model, are the followings: i) The TEG parameters analysed in Section 2, which include; S the Seebeck coefficient, 273.15 the absolute temperature in kelvin, T_{i1} fluid temperature of heatsink1, T_{i2} fluid temperature of heatsink2, if required the TEG configuration in series T_s and or in parallel T_p, r the TEG thermocouple p-n junction resistance, k the TEG thermocouple p-n junction thermal conductivity, ρ the TEG thermocouple p-n junction electrical resistivity, a the TEG thermocouple p-n junction area, L the TEG thermocouple p-n junction length and P_{req} the TEG total output power required. ii) The heatsinks parameters, which include; Ab the heatsink base area, n_1 fins efficiency of heatsink1, h_1 convection coefficient of heatsink1 fluid, A_1 total area of heatsink1 with fins sides, n_2 fins efficiency of heatsink2, h_2 convection coefficient of heatsink2 fluid and A_2 total area of heatsink2 with fins sides. All these parameters can easily be input in the model simulator and the TEG optimal parameters value computed as depicted in Figure 2.

Additionally, the TEG dimensionless parameters such as; N_i the dimensionless output current, N_k the dimensionless thermal conductance, Eff^* (n_{th}) the conversion efficiency, P_{os} (W_{s1}) the dimensionless output power, T_{s1} the TEG hot-side dimensionless temperature, T_{s2} the TEG cold-side dimensionless temperature and N_v the dimensionless output voltage, can all be either manually entered (as depicted in Figure 2 on the left side of the TEG with heatsinks model) or computed automatically. They're then used to finally calculate the TEG practical parameters values in SI units (as shown in Figure 2 on the right side of the TEG with heatsinks model). Some of the TEG physical parameters of interest that are computed include; Z the TEG figure of merit, n the TEG amount of p-n junction thermocouples, Q_h (Q_1) the TEG hot side heat absorbed, Q_c (Q_2) the TEG cold side heat released, P_o the TEG output power, T_1 (T_h) the TEG hot side temperature, T_2 (T_c) the TEG cold side temperature, R_R (R_t) the TEG internal resistance, V_o the TEG output voltage, V_{oc} is the TEG ideal output voltage, I the TEG output current, N the total amount of TEG modules required, DT or ΔT the TEG temperature difference and QPD is TEG with heatsinks heat flux density. The computed heatsinks parameters are: nhA the dimensionless convection conductance of heatsinks 1 or 2 fluid, T_{i1} and T_{i2} are fluids 1 and 2 hot and cold temperatures respectively, T_i the dimensionless fluid temperature, N_h the dimensionless convection conductance, ZT_{i2} the dimensionless figure of merit at T_{i2}, ZTA the TEG dimensionless figure of merit at TA. The TEG with heatsinks normalised, maximum and effective parameters are also computed.

In terms of the aesthetics, the TEG-HS output and inputs parameters were sorted together based on their commonalities, as well as labeled and colour coded accordingly to make the TEG with heatsinks model simple to comprehend and as well user friendly as shown in Figure 2.

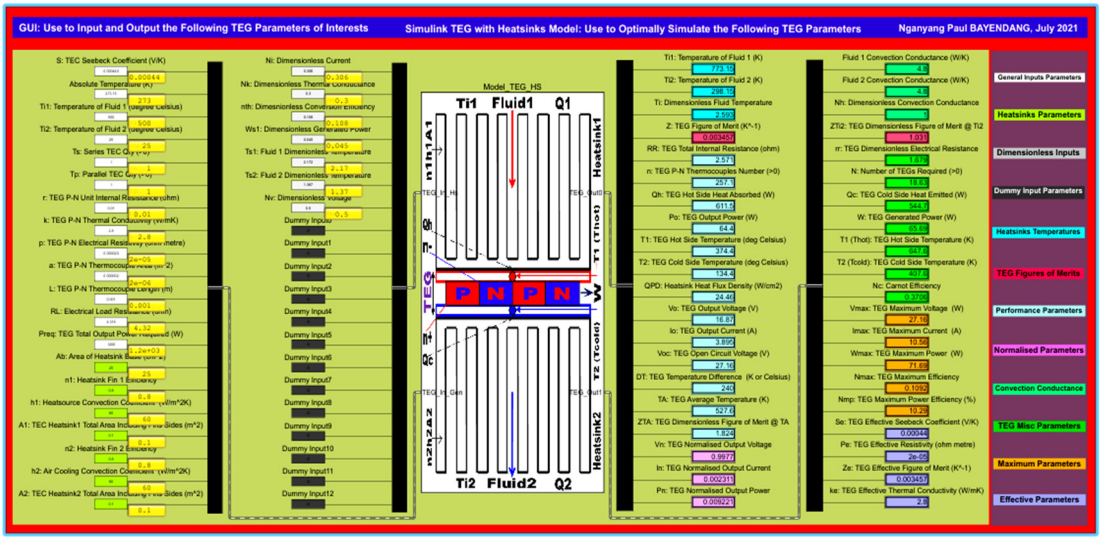

Figure 2. TEG with heatsinks model simulator.

Finally, in addition to the TEG with heatsinks numeric model computations, miscellaneous characteristics curves of some of the TEG crucial parameters of interest such as Q_{s1}, Q_{s2}, P_{os}, Eff^*, T_{s1} and T_{s2}; were plotted against N_k, R_r and DT_s to graphically calculate Q_{s1}, Q_{s2}, P_{os}, Eff^*,T_{s1} and T_{s2} different optimal values for $ZT_{i2} = 1$, $N_h = 1$, $T_i = 2.6$, $N_k = 0.1 - 0.4$, $R_r = 0.5 - 2$ and $DT_S = 0.1 - 1$. These graphical results are in details, variously demonstrated next in Figures 3 to 6 and with the highlights summarised in Table 1.

Table 1. Summary of the study comparing the "simple" and "simpler" equations results in Figures 3–6.

	R_r	N_k	DT_S	T_{s1}-T_{s2}	Q_{s1}	Q_{s2}	P_{os}	Eff^*	T_{s1}	T_{s2}
Using "Simple" Eqs 32 and 33	2	0.3	0.8	0.83564	0.404938	0.35942	0.045518	0.112407	2.19506	1.35942
	1.7	0.3	0.8	0.80401	0.420599	0.375429	0.0451302	0.10731	2.17944	1.37543
	1.1	0.3	0.8	0.7129	0.462515	0.424578	0.0379377	0.0820247	2.13748	1.42458
	1	0.3	0.8	0.69221	0.471429	0.436364	0.0350649	0.0743802	2.12857	1.43636
	0.5	0.3	0.8	0.54428	0.528736	0.526984	0.00175151	0.00331263	2.07126	1.52698
Using "Simpler" Eqs 36 and 37	2	0.3	0.8	0.83736	0.414815	0.347826	0.0669887	0.161491	2.18519	1.34783
	1.7	0.3	0.8	0.80637	0.432653	0.360976	0.0716775	0.16567	2.16735	1.36098
	1.1	0.3	0.8	0.71795	0.482051	0.4	0.0820513	0.170213	2.11795	1.4
	1	0.3	0.8	0.69805	0.492857	0.409091	0.0837662	0.16996	2.10714	1.40909
	0.5	0.3	0.8	0.55829	0.565517	0.47619	0.0893268	0.157956	2.03448	1.47619

4. Simulation results, discussions and validation

In Section 3, the TEG with heatsinks simulated model was presented with highlights on its various parameters and the numeric results, as exemplified in Figure 2 and summarised in Table 2. These results as well as the numerous graphical results displayed extensively next, are based on the new simple and simpler analytical T_{s1} and T_{s2} formulas derived in Section 2. These are comparatively engaged and displayed next and various comparisons of Q_{s1}, Q_{s2}, P_{os}, T_{s1}, T_{s2} and Eff^* with different combinations of ZT_{i2}, N_h T_i, N_k, R_r and DT_S using the simple Eqs 32 and 33 as well as using the simpler Eqs 36 and 37 are shown and organised as follows. i) all the figures on the left are based on using the simple Eqs 32 and 33 T_{s1} and T_{s2} values, whereas all the figures on the right are based on using the simpler Eqs 36 and 37 T_{s1} and T_{s2} values. ii) Figure 3 graphs depict Q_{s1}, Q_{s2}, P_{os}, T_{s1}, T_{s2}

and *Eff** results using $ZT_{i2} = 1$, $N_h = 1$, $T_i = 2.6$, $N_k = 0.1 - 0.4$, $R_r = 0 - 6$ and $DT_S = 0.8$. iii) Figure 4 graphs depict Q_{s1}, Q_{s2}, P_{os}, T_{s1}, T_{s2} and *Eff** results using $ZT_{i2} = 1$, $N_h = 1$, $T_i = 2.6$, $N_k = 0.05 - 0.5$, $R_r = 0.5 - 2$ and $DT_S = 0.8$. iv) Figure 5 graphs depict in 3D Q_{s1}, Q_{s2}, P_{os}, T_{s1}, T_{s2} and *Eff** results with $ZT_{i2} = 1$, $N_h = 1$, $T_i = 2.6$, $N_k = 0.3$, $R_r = 0.2 - 3.2$ and $DT_S = 0.1 - 1$. v) Figure 6 graphs depict in 3D Q_{s1}, Q_{s2}, P_{os}, T_{s1}, T_{s2} and *Eff** results using $ZT_{i2} = 1$, $N_h = 1$, $T_i = 2.6$, $N_k = 0.05 - 0.5$, $R_r = 1.7$ and $DT_S = 0.1 - 1$. Table 1 summarises the comparison of the simple Eqs 32 and 33 results and the simpler Eqs 36 and 37 results. Figures 2–6 results are also provided as supplementary picture files to enable every aspect of our findings to be viewed clearly in high quality without ambiguities.

Table 2. Summary of Figure 2 (TEG-HS model simulator) simulation results.

Input Parameters					Output Parameters			
TEG Parameters			Heatsinks Parameters		Heatsink Fluids Temps		Convection Conductances	
S	(V/K)	0.00044	Ab (W/cm^2)	25	T_{i1} (K)	773.15	$\eta_1 h_1 A_1$ (W/K)	4.8
Absolute T (K)		273.15	n_1	0.8	T_{i2} (K)	298.15	$\eta_2 h_2 A_2$ (W/K)	4.8
T_{i1}	(℃)	500	$h1$ (W/m^{2}K)	60	T_i	2.593	N_h	1
T_{i2}	(℃)	25	A_1 (m^2)	0.1	Figures of Merit		Dimensionless Heat Flows	
Ts		1	n_2	0.8	Z (K^{-1})	0.003457	Q_{s1}	0.420599
Tp		1	$h2$ (W/m^{2}K)	60	$ZTi2$	1.031	Q_{s2}	0.375429
R	(Ω)	0.01	A_2 (m^2)	0.1	TEG Practical Performance Parameters			
k	(W/mK)	2.8			RR (Ω)	2.571	Rr (rr)	1.679
ρ	(Ωm)	0.00002	Dimensionless Parameters		n	257.1	N	18.63
a	(m^2)	0.000002	N_i	0.306	Q_h (Q_1) (W)	611.5	Q_c (Q_2) (W)	544.7
L	(m)	0.001	N_k	0.3	Po (W)	64.4	W_n (W)	65.69
R_L	(Ω)	4.32	n_{th} (Eff^*)	0.108	T_1 (T_h) (℃)	374.4	T_1 (T_h) (K)	647.6
$Preq$	(W)	1200	$Ws1$ (Pos)	0.045	T_2 (T_c) (℃)	134.4	T_2 (T_c) (K)	407.6
			T_{s1}	2.172	QPD (W/cm^2)	24.46	Nc	0.3706
			T_{s1}	1.367	V_o (V)	16.87	V_{max} (V)	27.16
			Nv	0.5	I_o (A)	3.896	I_{max} (A)	10.56
			DTs	0.8	V_{oc} (V)	27.16	W_{max} (W)	71.69
			NB: the dimensionless parameters here can both be inputs and outputs		ΔT (℃)	240	N_{max}	0.1092
					TA (℃)	527.6	Nmp_{max} (%)	10.29
					ZTA (℃)	1.824	ΔT (K)	240

Figure 3 graphs depict Q_{s1}, Q_{s2}, P_{os}, T_{s1}, T_{s2} and *Eff** results using $ZT_{i2} = 1$, $N_h = 1$, $T_i = 2.6$, $N_k = 0.1 - 0.4$, $R_r = 0 - 6$ and $DT_S = 0.8$. It also compares the newly introduced simple vs simpler equations results.

$N_k = 0.1 - 0.4$: Using "simple" Eqs 32 and 33

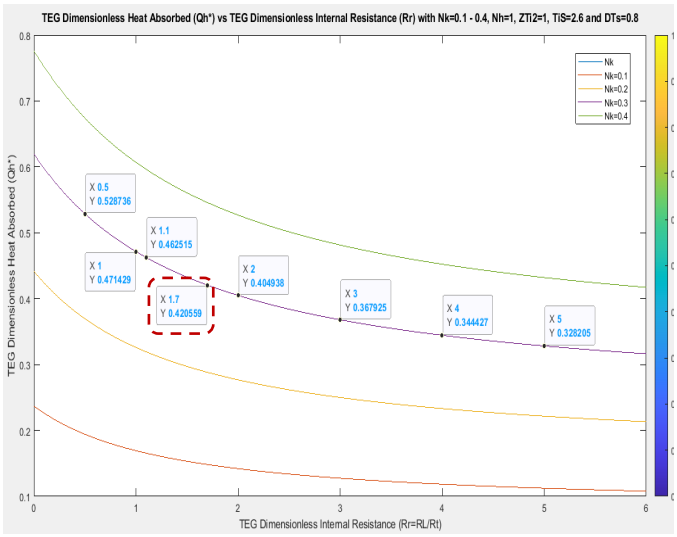

(a)

$N_k = 0.1 - 0.4$: Using "simpler" Eqs 36 and 37

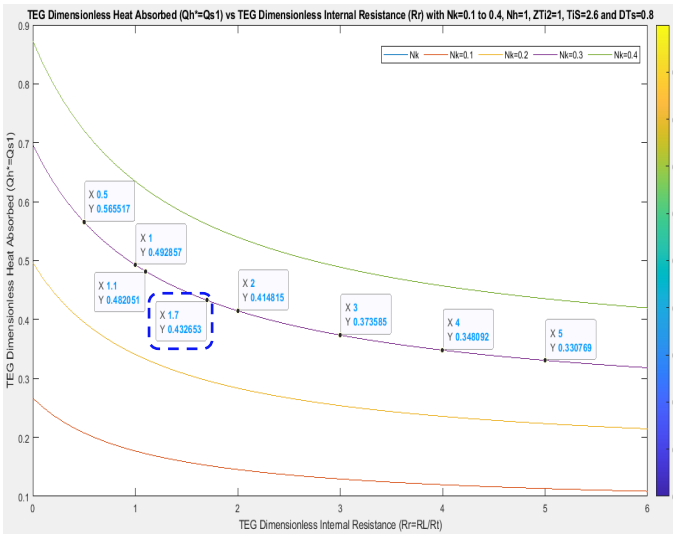

(g)

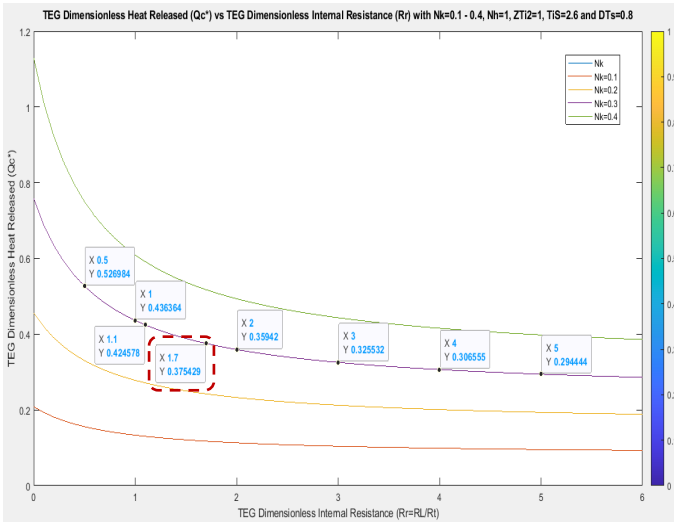

(b)

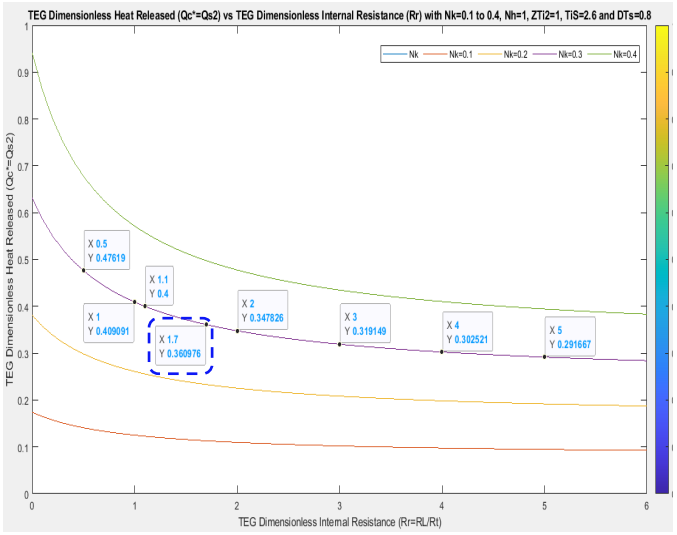

(h)

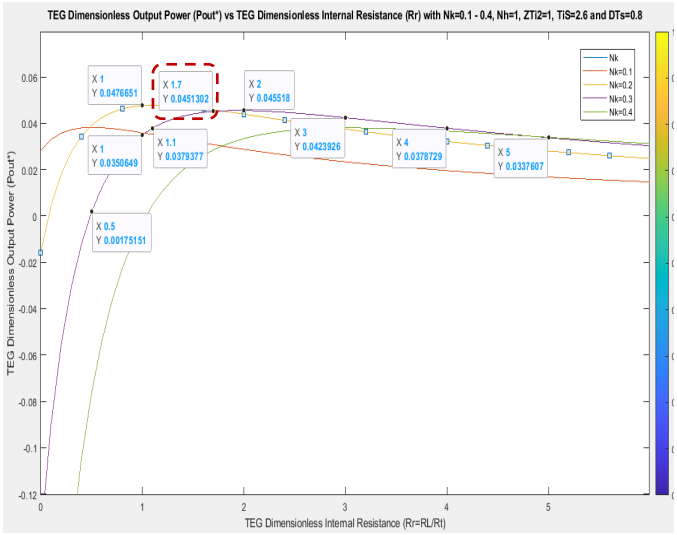
TEG Dimensionless Output Power (Pout*) vs TEG Dimensionless Internal Resistance (Rr) with Nk=0.1 - 0.4, Nh=1, ZTi2=1, TiS=2.6 and DTs=0.8
TEG Dimensionless Output Power (Pout*)
TEG Dimensionless Internal Resistance (Rr=RL/Rt)
Nk
Nk=0.1
Nk=0.2
Nk=0.3
Nk=0.4
X 1
Y 0.0476651
X 1.7
Y 0.0451302
X 2
Y 0.045518
X 3
Y 0.0423926
X 4
Y 0.0378729
X 5
Y 0.0337607
X 1.1
Y 0.0379377
X 1
Y 0.0350649
X 0.5
Y 0.00175151

(c)

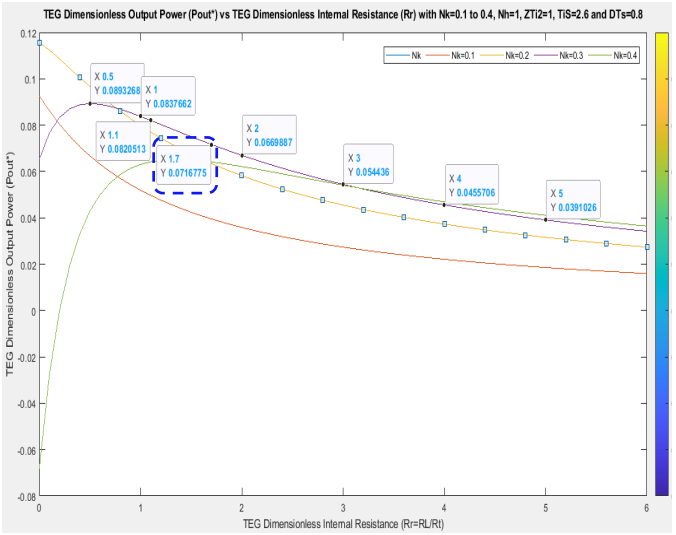
TEG Dimensionless Output Power (Pout*) vs TEG Dimensionless Internal Resistance (Rr) with Nk=0.1 to 0.4, Nh=1, ZTi2=1, TiS=2.6 and DTs=0.8
TEG Dimensionless Output Power (Pout*)
TEG Dimensionless Internal Resistance (Rr=RL/Rt)
Nk
Nk=0.1
Nk=0.2
Nk=0.3
Nk=0.4
X 0.5
Y 0.0893268
X 1
Y 0.0837662
X 1.1
Y 0.0820513
X 1.7
Y 0.0716775
X 2
Y 0.0669887
X 3
Y 0.054436
X 4
Y 0.0455706
X 5
Y 0.0391026

(i)

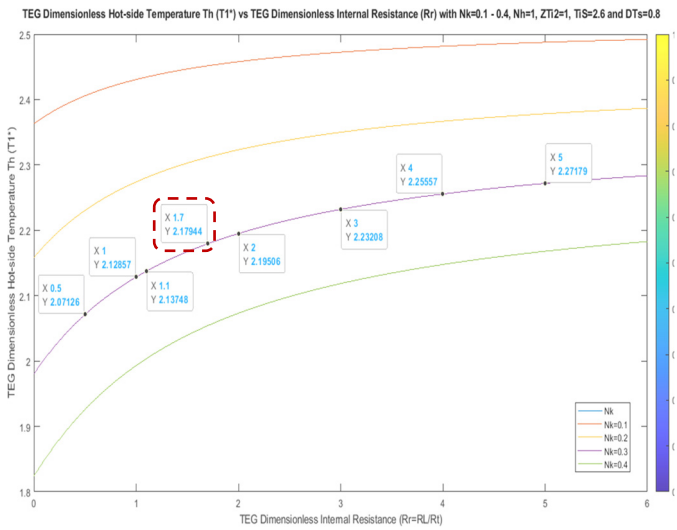
TEG Dimensionless Hot-side Temperature Th (T1*) vs TEG Dimensionless Internal Resistance (Rr) with Nk=0.1 - 0.4, Nh=1, ZTi2=1, TiS=2.6 and DTs=0.8
TEG Dimensionless Hot-side Temperature Th (T1*)
TEG Dimensionless Internal Resistance (Rr=RL/Rt)
Nk
Nk=0.1
Nk=0.2
Nk=0.3
Nk=0.4
X 1.7
Y 2.17944
X 4
Y 2.25557
X 5
Y 2.27179
X 3
Y 2.23208
X 2
Y 2.19506
X 1
Y 2.12857
X 1.1
Y 2.13748
X 0.5
Y 2.07126

(d)

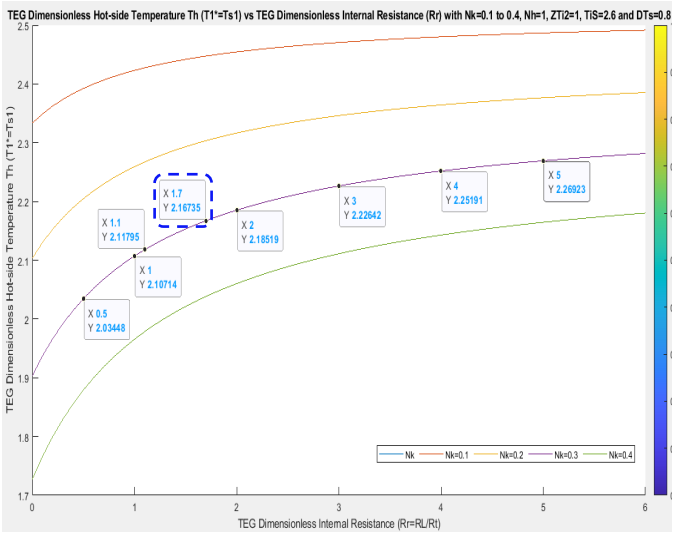
TEG Dimensionless Hot-side Temperature Th (T1*=Ts1) vs TEG Dimensionless Internal Resistance (Rr) with Nk=0.1 to 0.4, Nh=1, ZTi2=1, TiS=2.6 and DTs=0.8
TEG Dimensionless Hot-side Temperature Th (T1*=Ts1)
TEG Dimensionless Internal Resistance (Rr=RL/Rt)
Nk
Nk=0.1
Nk=0.2
Nk=0.3
Nk=0.4
X 1.7
Y 2.16735
X 1.1
Y 2.11795
X 2
Y 2.18519
X 3
Y 2.22642
X 4
Y 2.25191
X 5
Y 2.26923
X 1
Y 2.10714
X 0.5
Y 2.03448

(j)

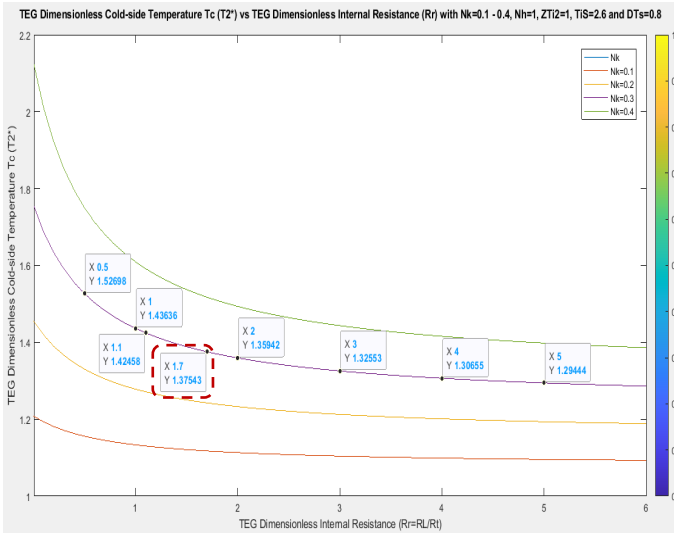

(e)

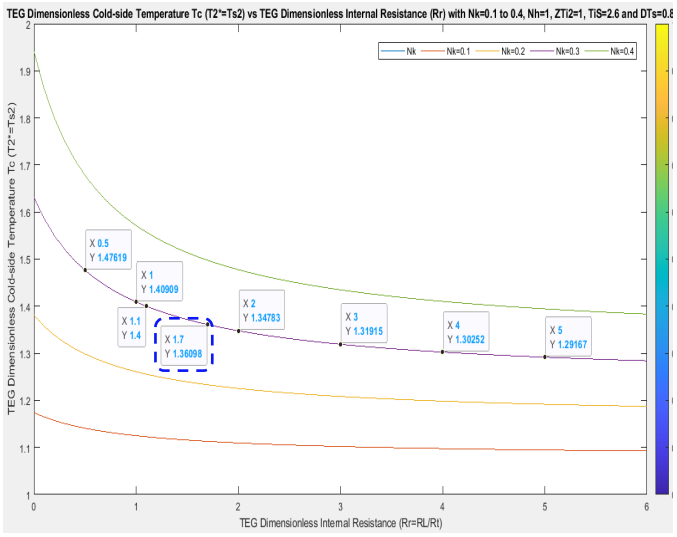

(k)

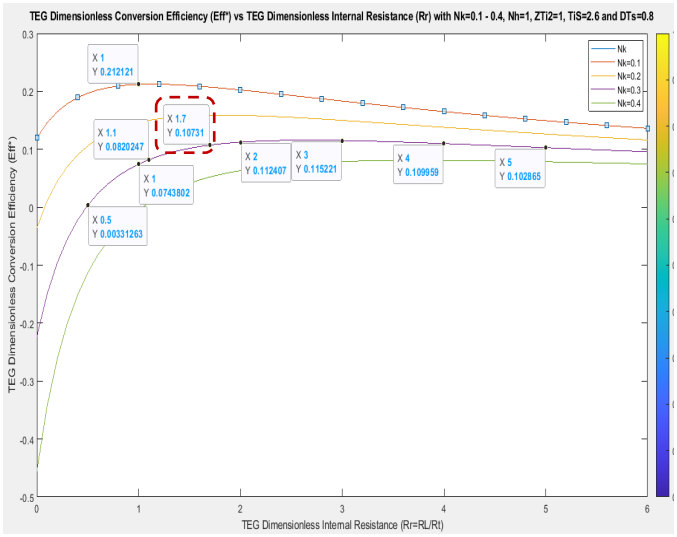

(f)

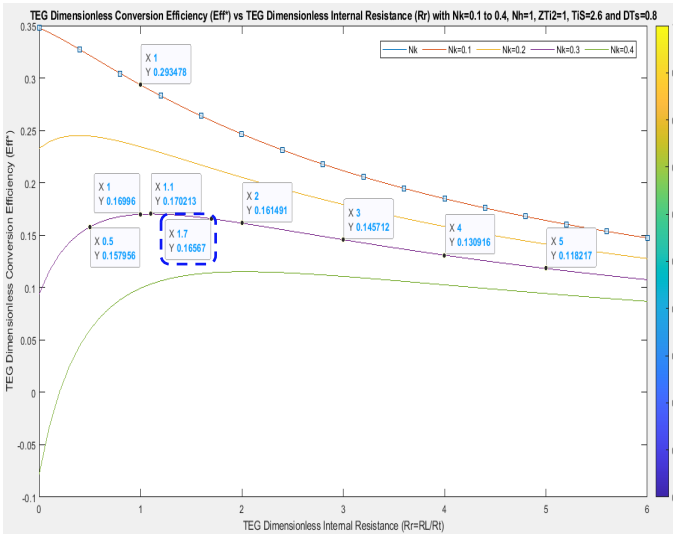

(l)

Figure 3. Performance and comparison plots of the: i) simple Eqs 32 and 33; (a) Q_{s1} vs R_r @N_k = 0.1 − 0.4; (b) Q_{s2} vs R_r @N_k = 0.1 − 0.4; (c) P_{os} vs R_r @N_k = 0.1 − 0.4; (d) T_{s1} vs R_r @N_k = 0.1 − 0.4; (e) T_{s2} vs R_r @N_k = 0.1 − 0.4; (f) *Eff** vs R_r @N_k = 0.1 − 0.4; ii) versus simpler Eqs 36 and 37; (g) Q_{s1} vs R_r @N_k = 0.1 − 0.4; (h) Q_{s2} vs R_r @N_k = 0.1 − 0.4; (i) P_{os} vs R_r @N_k = 0.1 − 0.4; (j) T_{s1} vs R_r @N_k = 0.1 − 0.4; (k) T_{s2} vs R_r @N_k = 0.3; (l) *Eff** vs R_r @N_k = 0.1 − 0.4.

Figure 4 graphs depict Q_{s1}, Q_{s2}, P_{os}, T_{s1}, T_{s2} and *Eff** results using ZT_{i2} = 1, N_h = 1, T_i = 2.6, N_k = 0.05 − 0.5, R_r = 0.5 − 2 and DT_S = 0.8. It also compares the newly introduced simple vs simpler formulas results.

$R_r = 0.5 - 2$: Using "simple" Eqs 32 and 33

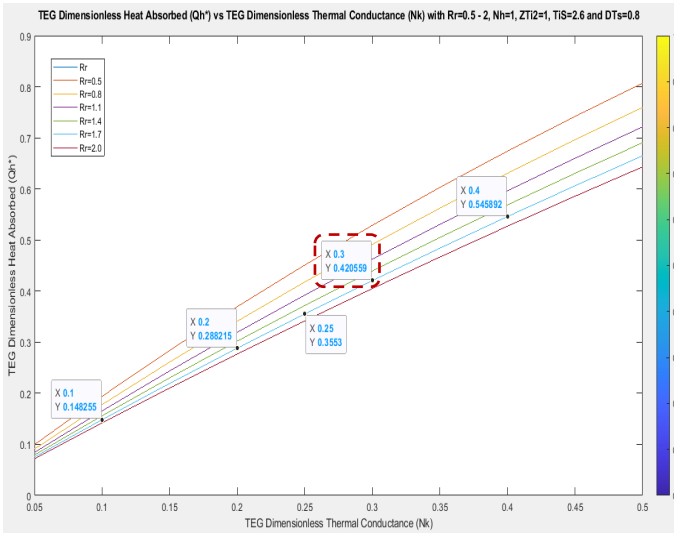

(a)

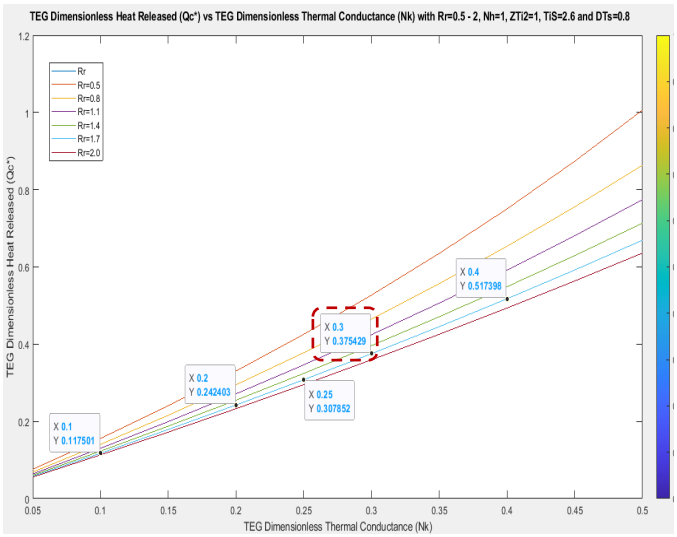

(b)

$R_r = 0.5 - 2$: Using "simpler" Eqs 36 and 37

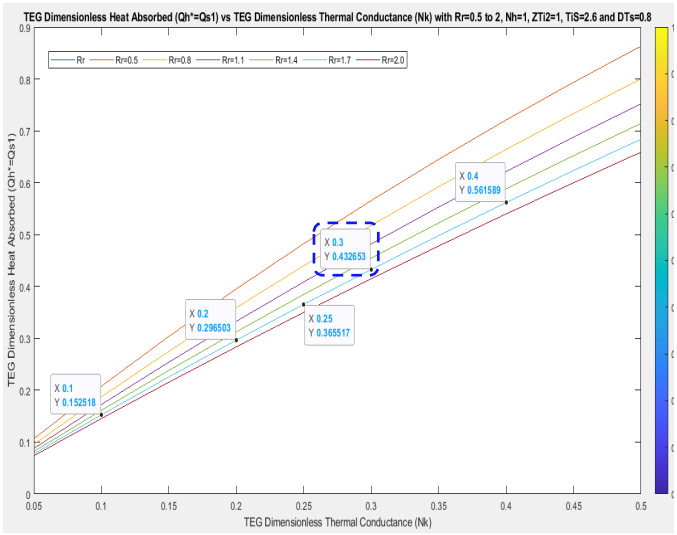

(g)

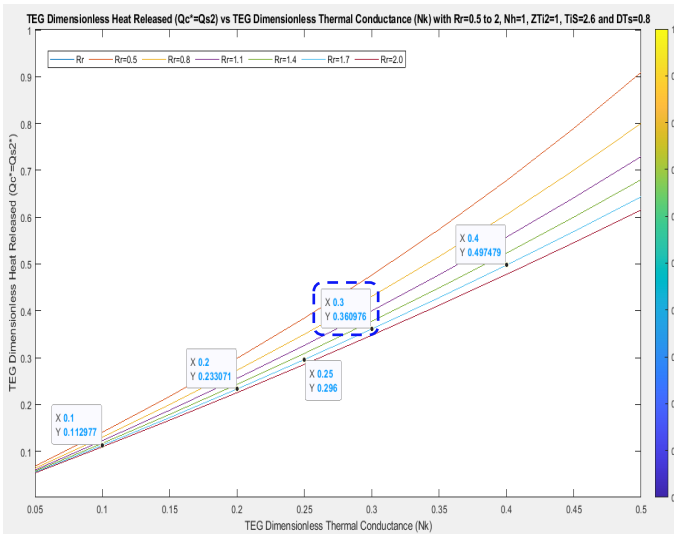

(h)

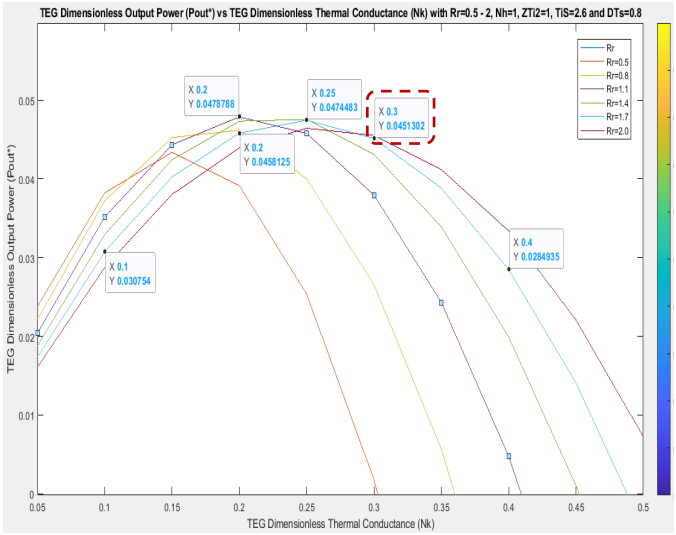
TEG Dimensionless Output Power (Pout*) vs TEG Dimensionless Thermal Conductance (Nk) with Rr=0.5 - 2, Nh=1, ZTi2=1, TiS=2.6 and DTs=0.8
TEG Dimensionless Output Power (Pout*)
TEG Dimensionless Thermal Conductance (Nk)
Rr
Rr=0.5
Rr=0.8
Rr=1.1
Rr=1.4
Rr=1.7
Rr=2.0
X 0.2
Y 0.0478788
X 0.25
Y 0.0474483
X 0.3
Y 0.0451302
X 0.2
Y 0.0458125
X 0.1
Y 0.030754
X 0.4
Y 0.0284935

(c)

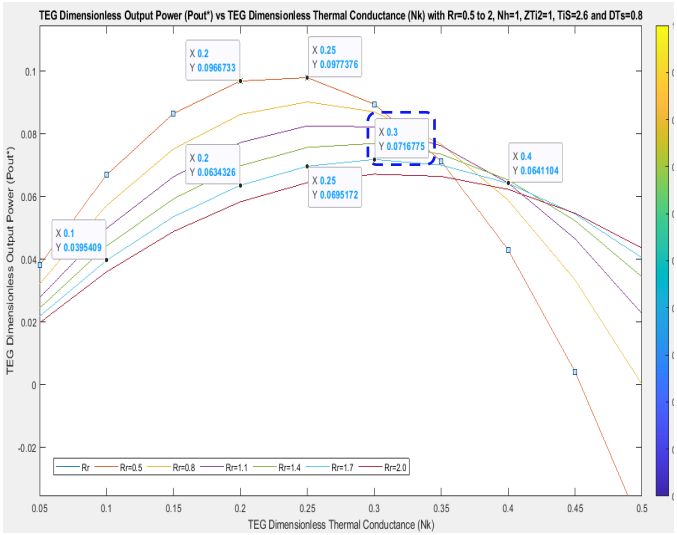
TEG Dimensionless Output Power (Pout*) vs TEG Dimensionless Thermal Conductance (Nk) with Rr=0.5 to 2, Nh=1, ZTi2=1, TiS=2.6 and DTs=0.8
TEG Dimensionless Output Power (Pout*)
TEG Dimensionless Thermal Conductance (Nk)
Rr
Rr=0.5
Rr=0.8
Rr=1.1
Rr=1.4
Rr=1.7
Rr=2.0
X 0.2
Y 0.0966733
X 0.25
Y 0.0977376
X 0.3
Y 0.0716775
X 0.2
Y 0.0634326
X 0.4
Y 0.0641104
X 0.25
Y 0.0695172
X 0.1
Y 0.0395409

(i)

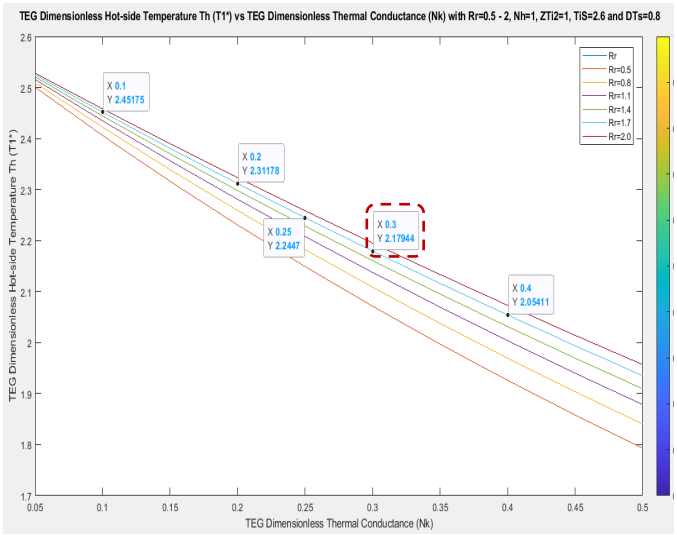
TEG Dimensionless Hot-side Temperature Th (T1*) vs TEG Dimensionless Thermal Conductance (Nk) with Rr=0.5 - 2, Nh=1, ZTi2=1, TiS=2.6 and DTs=0.8
TEG Dimensionless Hot-side Temperature Th (T1*)
TEG Dimensionless Thermal Conductance (Nk)
Rr
Rr=0.5
Rr=0.8
Rr=1.1
Rr=1.4
Rr=1.7
Rr=2.0
X 0.1
Y 2.45175
X 0.2
Y 2.31178
X 0.25
Y 2.2447
X 0.3
Y 2.17944
X 0.4
Y 2.05411

(d)

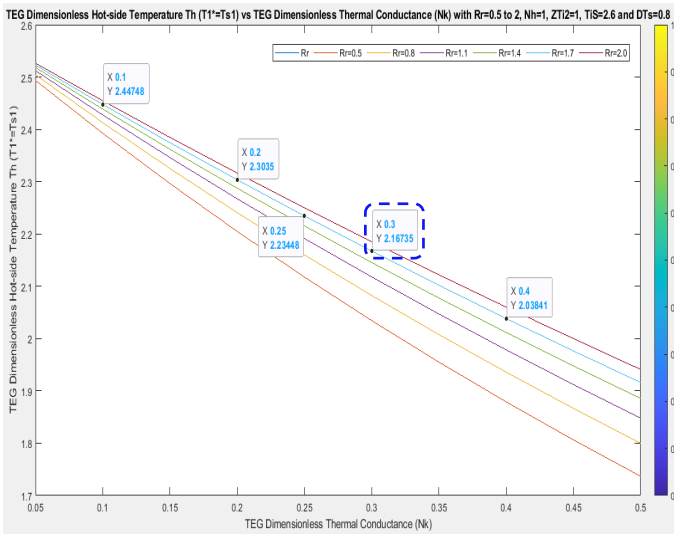
TEG Dimensionless Hot-side Temperature Th (T1*=Ts1) vs TEG Dimensionless Thermal Conductance (Nk) with Rr=0.5 to 2, Nh=1, ZTi2=1, TiS=2.6 and DTs=0.8
TEG Dimensionless Hot-side Temperature Th (T1*=Ts1)
TEG Dimensionless Thermal Conductance (Nk)
Rr
Rr=0.5
Rr=0.8
Rr=1.1
Rr=1.4
Rr=1.7
Rr=2.0
X 0.1
Y 2.44748
X 0.2
Y 2.3035
X 0.25
Y 2.23448
X 0.3
Y 2.16735
X 0.4
Y 2.03841

(j)

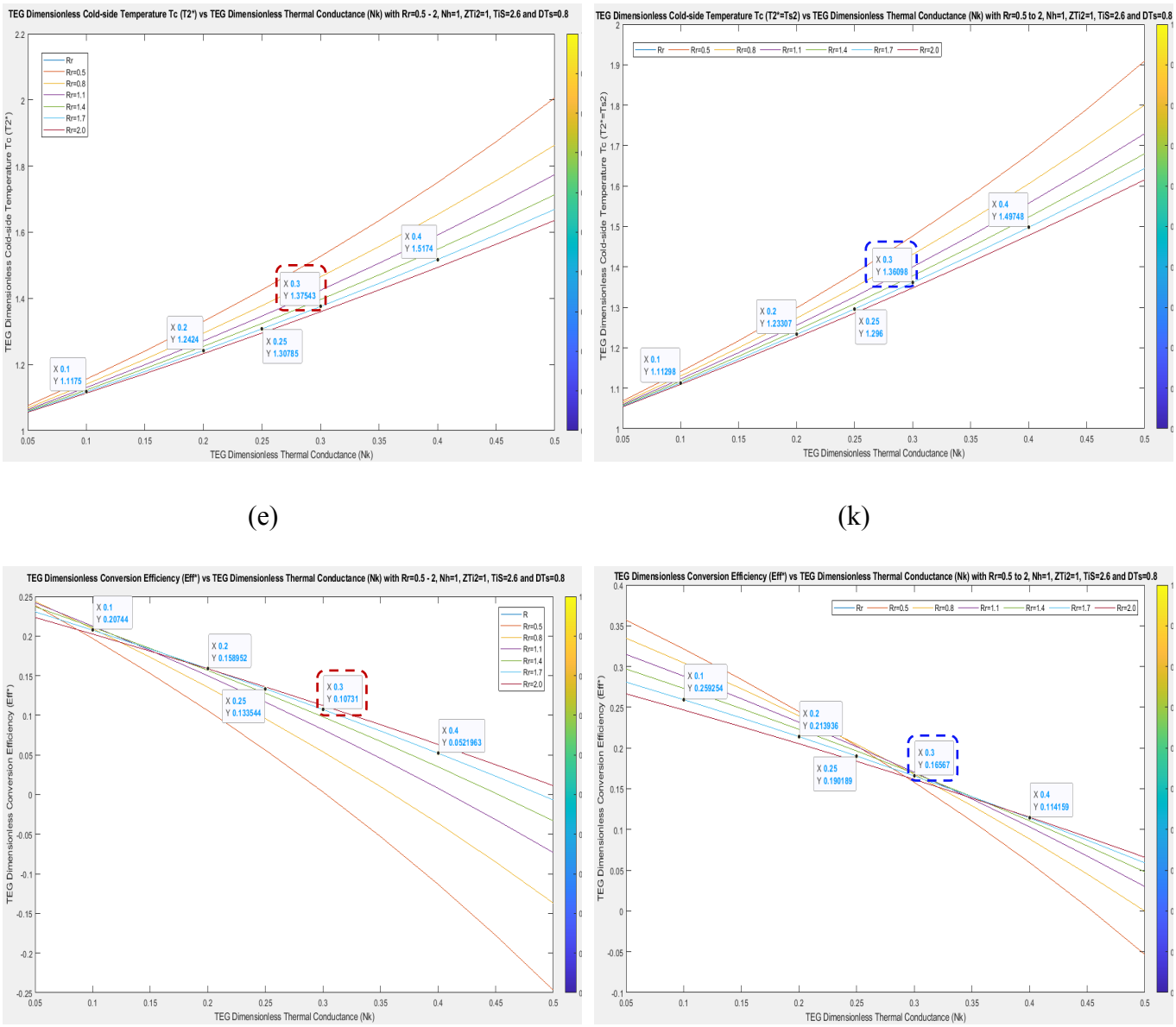

(e) (k)

(f) (l)

Figure 4. Performance and comparison plots of the: i) simple Eqs 32 and 33; (a) Q_{s1} vs N_k @ $R_r = 0.5 - 2$; (b) Q_{s2} vs N_k @ $R_r = 0.5 - 2$; (c) P_{os} vs N_k @ $R_r = 0.5 - 2$; (d) T_{s1} vs N_k @ $R_r = 0.5 - 2$; (e) T_{s2} vs N_k @$R_r = 0.5 - 2$; (f) *Eff** vs N_k @ $R_r = 0.5 - 2$; versus ii) simpler Eqs 36 and 37; (g) Q_{s1} vs N_k @$R_r = 0.5 - 2$; (h) Q_{s2} vs N_k @ $R_r = 0.5 - 2$; (i) P_{os} vs N_k @ $R_r = 0.5 - 2$; (j) T_{s1} vs N_k @ $R_r = 0.5 - 2$; (k) T_{s2} vs N_k @ $R_r = 0.5 - 2$; (l) *Eff** vs N_k @ $R_r = 0.5 - 2$.

Figure 5 graphs depict in 3D Q_{s1}, Q_{s2}, P_{os}, T_{s1}, T_{s2} and *Eff** results with $ZT_{i2} = 1$, $N_h = 1$, $T_i = 2.6$, $N_k = 0.3$, $R_r = 0.2 - 3.2$ and $DT_S = 0.1 - 1$. The newly introduced simple vs simpler equations results are also correlated.

R_r vs DT_s: Using “simple” Eqs 32 and 33

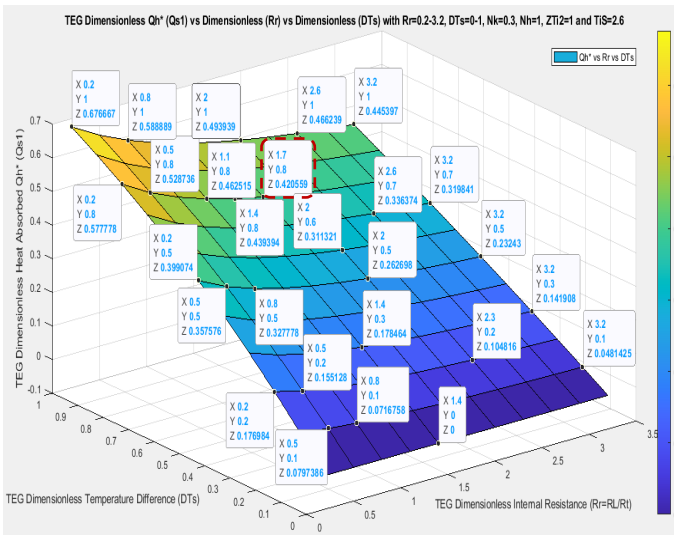

(a)

Rr vs DTs: Using “simpler” Eqs 36 and 37

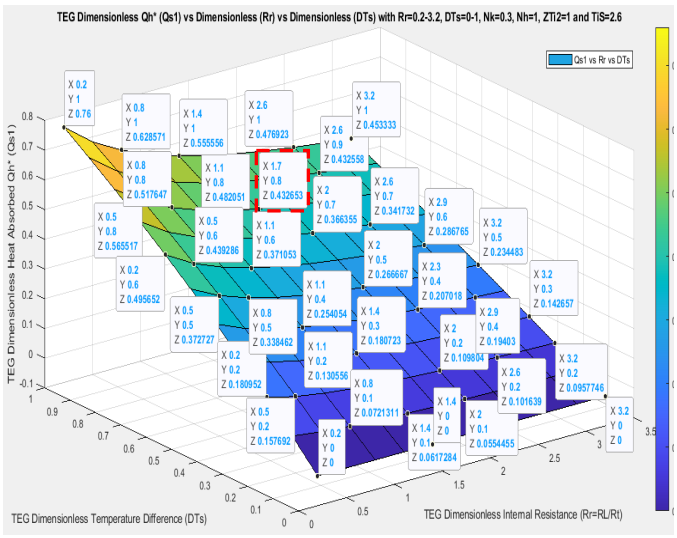

(g)

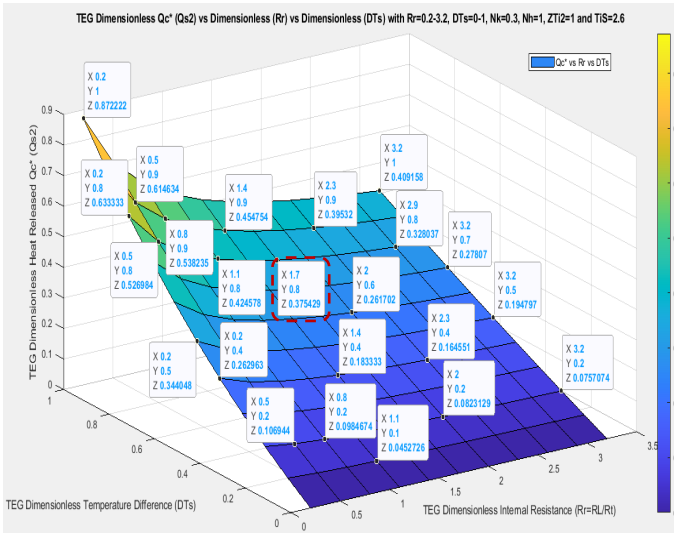

(b)

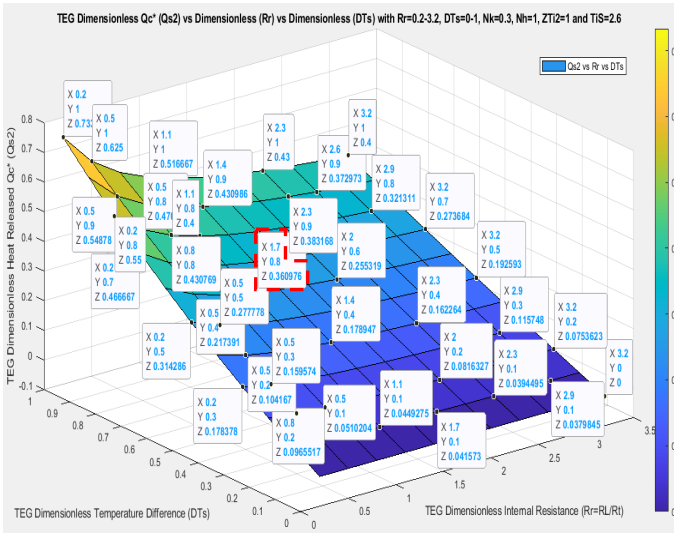

(h)

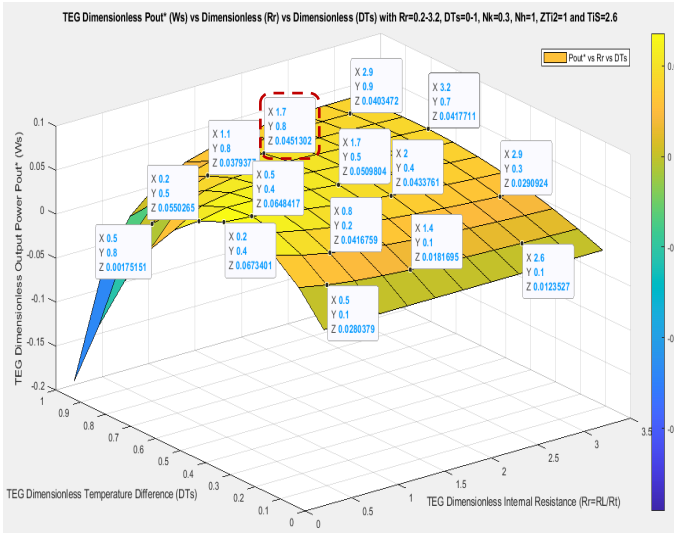
TEG Dimensionless Pout* (Ws) vs Dimensionless (Rr) vs Dimensionless (DTs) with Rr=0.2-3.2, DTs=0-1, Nk=0.3, Nh=1, ZTi2=1 and TiS=2.6
Pout* vs Rr vs DTs
TEG Dimensionless Output Power Pout* (Ws)
TEG Dimensionless Temperature Difference (DTs)
TEG Dimensionless Internal Resistance (Rr=RL/Rt)

(c)

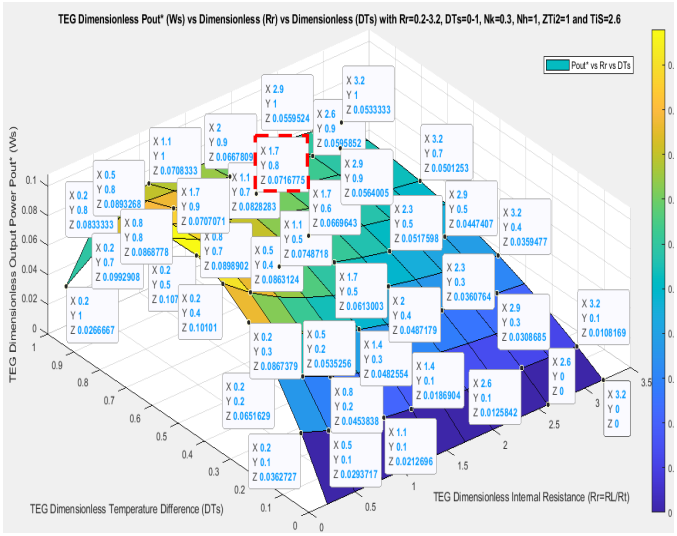
TEG Dimensionless Pout* (Ws) vs Dimensionless (Rr) vs Dimensionless (DTs) with Rr=0.2-3.2, DTs=0-1, Nk=0.3, Nh=1, ZTi2=1 and TiS=2.6
Pout* vs Rr vs DTs
TEG Dimensionless Output Power Pout* (Ws)
TEG Dimensionless Temperature Difference (DTs)
TEG Dimensionless Internal Resistance (Rr=RL/Rt)

(i)

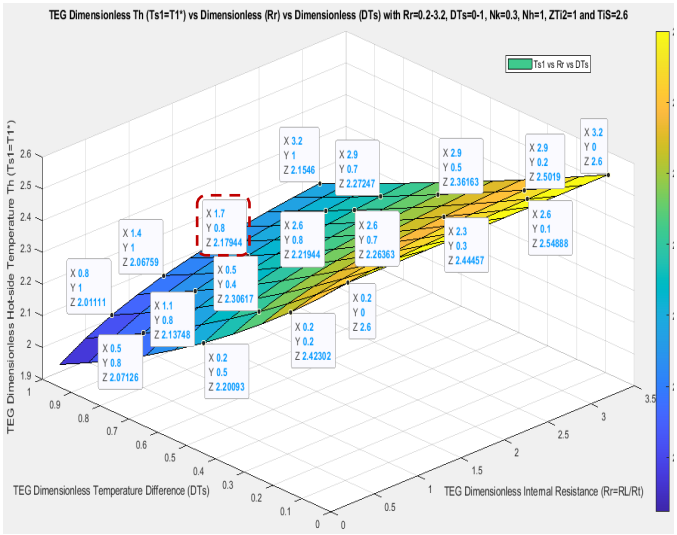
TEG Dimensionless Th (Ts1=T1*) vs Dimensionless (Rr) vs Dimensionless (DTs) with Rr=0.2-3.2, DTs=0-1, Nk=0.3, Nh=1, ZTi2=1 and TiS=2.6
Ts1 vs Rr vs DTs
TEG Dimensionless Hot-side Temperature Th (Ts1=T1*)
TEG Dimensionless Temperature Difference (DTs)
TEG Dimensionless Internal Resistance (Rr=RL/Rt)

(d)

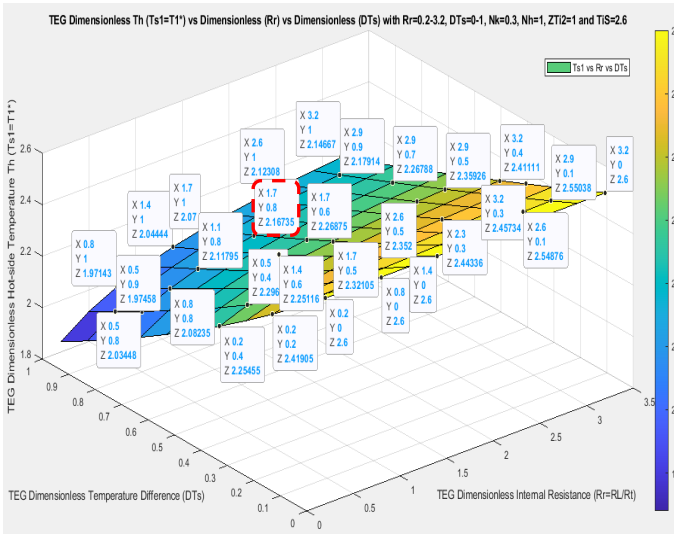
TEG Dimensionless Th (Ts1=T1*) vs Dimensionless (Rr) vs Dimensionless (DTs) with Rr=0.2-3.2, DTs=0-1, Nk=0.3, Nh=1, ZTi2=1 and TiS=2.6
Ts1 vs Rr vs DTs
TEG Dimensionless Hot-side Temperature Th (Ts1=T1*)
TEG Dimensionless Temperature Difference (DTs)
TEG Dimensionless Internal Resistance (Rr=RL/Rt)

(j)

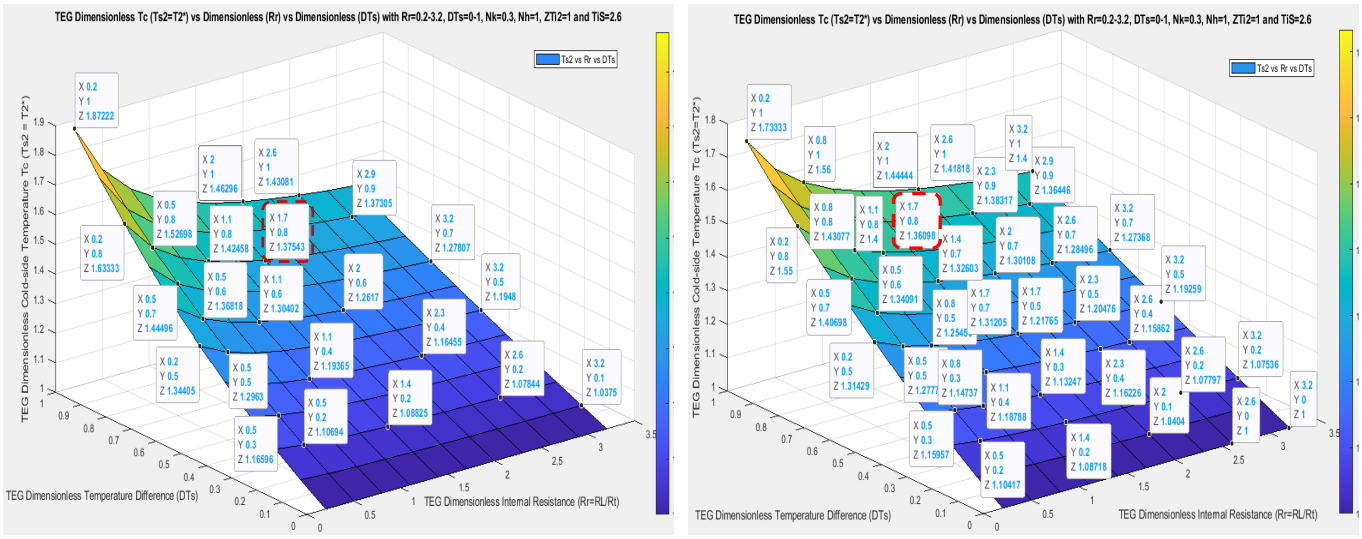

(e) (k)

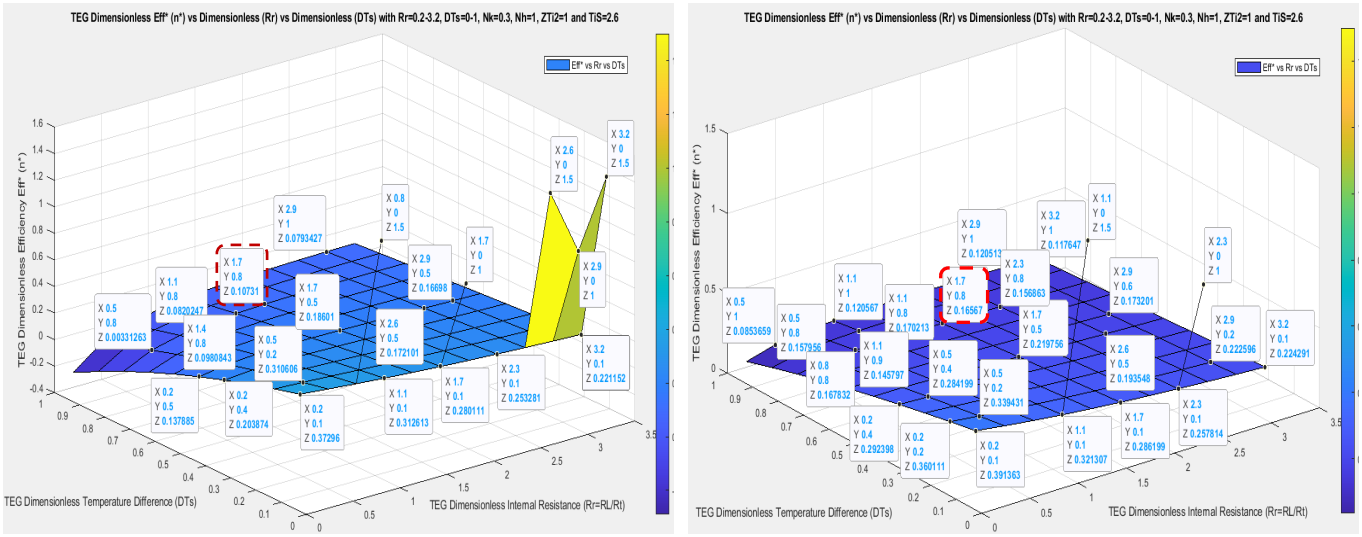

(f) (l)

Figure 5. Performance and comparison plots of the: i) simple Eqs 32 and 33; (a) Q_{s1} vs R_r vs DT_s; (b) Q_{s2} vs R_r vs DT_s; (c) P_{os} vs R_r vs DT_s; (d) T_{s1} vs R_r vs DT_s; (e) T_{s2} vs R_r vs DT_s; (f) Eff^* vs R_r vs DT_s; versus ii) simpler Eqs 36 and 37; (g) Q_{s1} vs R_r vs DT_s; (h) Q_{s2} vs R_r vs DT_s; (i) P_{os} vs R_r vs DT_s ; (j) T_{s1} vs R_r vs DT_s ; (k) T_{s2} vs R_r vs DT_s; (l) Eff^* vs R_r vs DT_s.

Figure 6 graphs depict in 3D Q_{s1}, Q_{s2}, P_{os}, T_{s1}, T_{s2} and Eff^* results using $ZT_{i2} = 1$, $N_h = 1$, $T_i = 2.6$, $N_k = 0.05 - 0.5$, $R_r = 1.7$ and $DT_S = 0.1 - 1$. The newly introduced simple vs simpler formulas results are compared.

N_k vs DT_s: Using “simple” Eqs 32 and 33

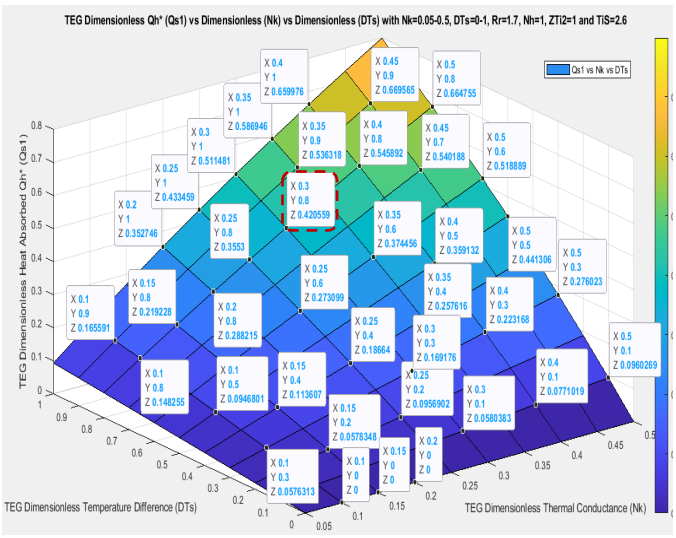

(a)

N_k vs DT_s: Using “simpler” Eqs 36 and 37

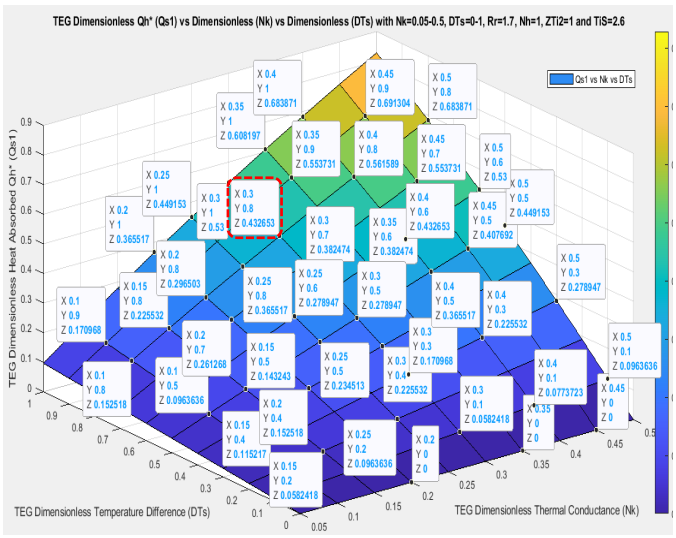

(g)

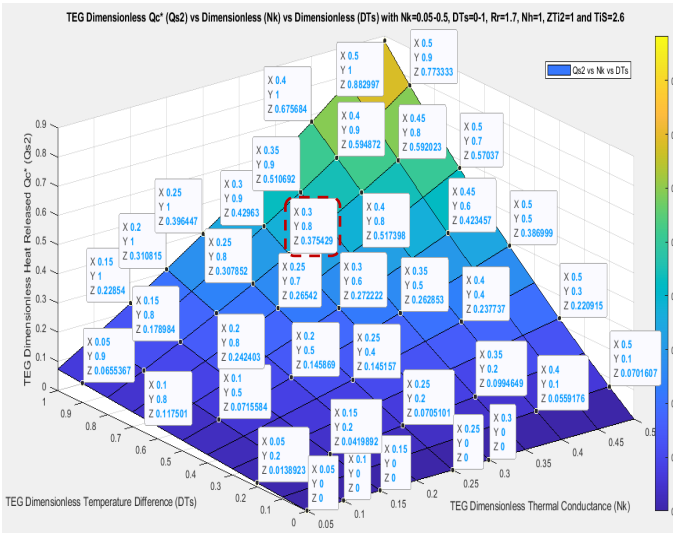

(b)

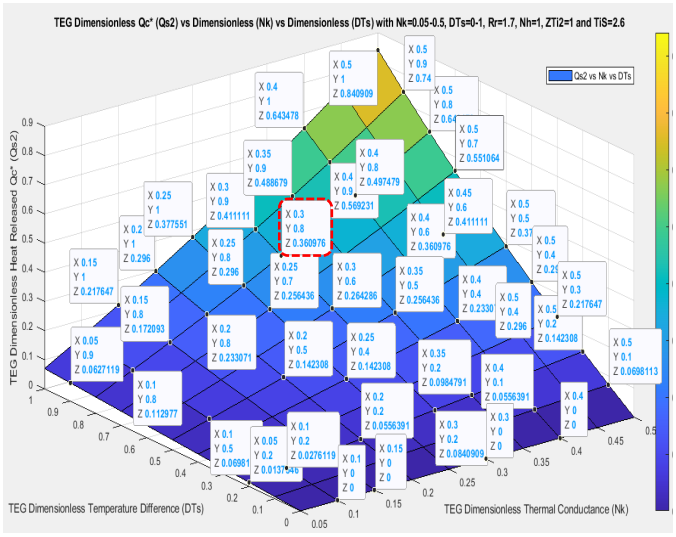

(h)

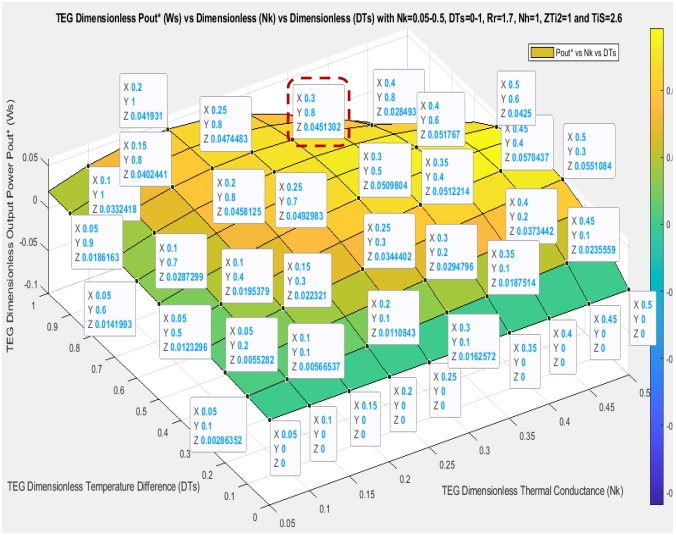
TEG Dimensionless Pout* (Ws) vs Dimensionless (Nk) vs Dimensionless (DTs) with Nk=0.05-0.5, DTs=0-1, Rr=1.7, Nh=1, ZTi2=1 and TiS=2.6
Pout* vs Nk vs DTs
TEG Dimensionless Output Power Pout* (Ws)
TEG Dimensionless Temperature Difference (DTs)
TEG Dimensionless Thermal Conductance (Nk)

(c)

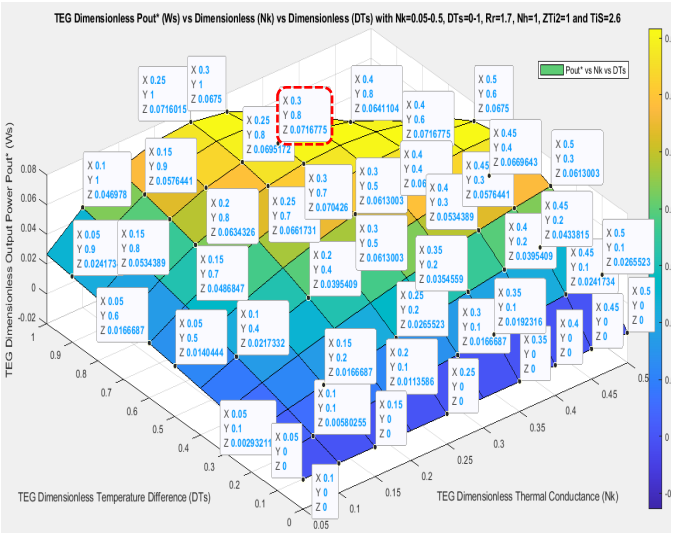
TEG Dimensionless Pout* (Ws) vs Dimensionless (Nk) vs Dimensionless (DTs) with Nk=0.05-0.5, DTs=0-1, Rr=1.7, Nh=1, ZTi2=1 and TiS=2.6
Pout* vs Nk vs DTs
TEG Dimensionless Output Power Pout* (Ws)
TEG Dimensionless Temperature Difference (DTs)
TEG Dimensionless Thermal Conductance (Nk)

(i)

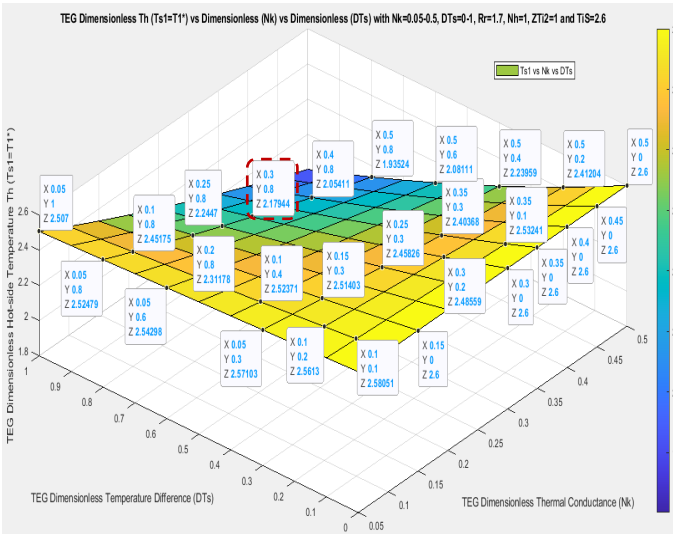
TEG Dimensionless Th (Ts1=T1*) vs Dimensionless (Nk) vs Dimensionless (DTs) with Nk=0.05-0.5, DTs=0-1, Rr=1.7, Nh=1, ZTi2=1 and TiS=2.6
Ts1 vs Nk vs DTs
TEG Dimensionless Hot-side Temperature Th (Ts1=T1*)
TEG Dimensionless Temperature Difference (DTs)
TEG Dimensionless Thermal Conductance (Nk)

(d)

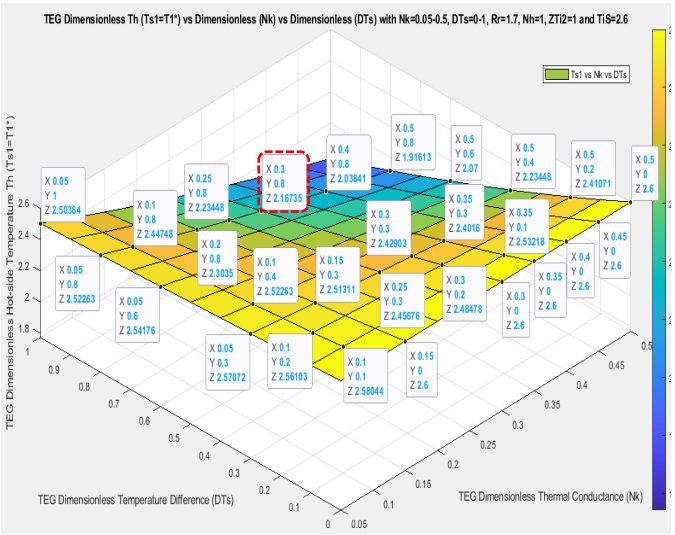
TEG Dimensionless Th (Ts1=T1*) vs Dimensionless (Nk) vs Dimensionless (DTs) with Nk=0.05-0.5, DTs=0-1, Rr=1.7, Nh=1, ZTi2=1 and TiS=2.6
Ts1 vs Nk vs DTs
TEG Dimensionless Hot-side Temperature Th (Ts1=T1*)
TEG Dimensionless Temperature Difference (DTs)
TEG Dimensionless Thermal Conductance (Nk)

(j)

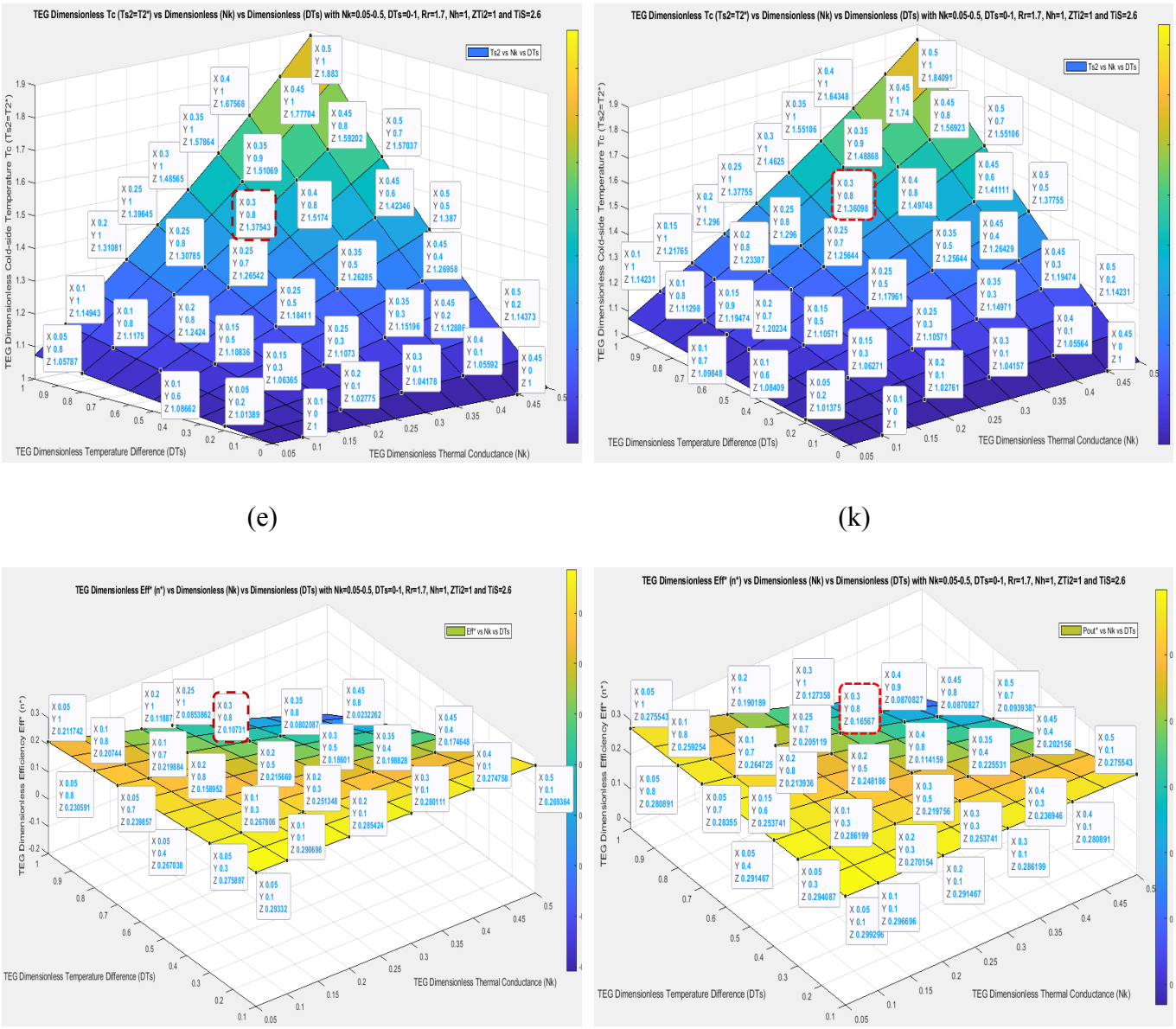

Figure 6. Performance and comparison plots of the: i) simple Eqs 32 and 33; (a) Q_{s1} vs N_k vs DT_s; (b) Q_{s2} vs N_k vs DT_s; (c) P_{os} vs N_k vs DT_s; (d) T_{s1} vs N_k vs DT_s; (e) T_{s2} vs N_k vs DT_s; (f) Eff^* vs N_k vs DT_s ; versus ii) simpler Eqs 36 and 37; (g) Q_{s1} vs N_k vs DT_s; (h) Q_{s2} vs N_k vs DT_s; (i) P_{os} vs N_k vs DT_s; (j) T_{s1} vs N_k vs DT_s; (k) T_{s2} vs N_k vs DT_s; (l) Eff^* vs N_k vs DT_s.

In the first part of Section 4, the study results were variously and extensively displayed, revealing what combinations of R_r vs N_k vs DT_s values that will give optimal Q_{s1}, Q_{s2}, P_{os}, T_{s1}, T_{s2} and Eff^* outcomes; by employing our newly introduced analytical Eqs 32 and 33 which are termed the "simple equations" and comparing with the further simplified versions, Eqs 36 and 37 which as well are termed the "simpler equations". It should be noted that each set of figures results, validate each

other set of figures results. That is, Figure 3 results validates Figure 4 results which in turn validates Figure 5 results and consequently which validates Figure 6 results. Furthermore, the figures on the left results (based on Eqs 32 and 33 exclusively) validate the figures on the right results (based on Eqs 36 and 37 exclusively). In the second part of Section 4, the highlights of our presented findings are discussed next and lastly the results are validated where applicable with reference to the original results presented in [7].

Beginning with Figure 3, parameters Q_{s1}, Q_{s2}, P_{os}, T_{s1}, T_{s2} and Eff* are plotted against R_r with $N_k = 0.1 - 0.4$ and $DT_s = 0.8$ as well as $ZT_{i2} = 1$, $N_h = 1$, $T_i = 2.6$—which were fixed throughout our entire study and therefore have no relevance in our results/discussions. NB: $N_k = 0.1 - 0.4$ instead of just $N_k = 0.3$ was used to see the effects of different N_k values on Q_{s1}, Q_{s2}, P_{os}, T_{s1}, T_{s2} and Eff* at also different R_r values. As evident, Q_{s1}, Q_{s2} and T_{s2} are inversely proportional to R_r with $N_k = 0.3$ and $DT_s = 0.8$. T_{s1} is directly proportional to R_r whereas P_{os} and Eff* are initially directly proportional to R_r, until P_{os} and Eff* reach their respective maximum value and then becomes inversely proportional to R_r and also with the rates of P_{os} and Eff* incline and decline, being faster using the "simpler" Eqs 36 and 37. With the "simple" equations, our optimal values for P_{os} is 0.045518 and for Eff* is 0.112407 and both occur at approximately $R_r = 2$ and not at exactly $R_r = 1.7$ as reported in [7]; however, at $R_r = 1.7$, our P_{os} and Eff* values of 0.0451302 and 0.10731 respectively, are exactly the same as those reported in [7]. With the "simpler" equations, our optimal values for P_{os} is 0.0893268 and for Eff* is 0.170213 and both occur at different R_r values—at $R_r = 0.5$ for P_{os} and at $R_r = 1.1$ for Eff*; however, at $R_r = 1.7$, both the P_{os} and Eff* values are respectively 0.0716775 and 0.16567, as well as respectively 0.0669887 and 0.161491 at $R_r = 2$. The rest parameters Q_{s1}, Q_{s2}, T_{s1} and T_{s2} values are closely the same using either the "simple" or "simpler" analytical equations. Further observable, the results dynamics have the following interesting aspects. i) Q_{s1}, Q_{s2} and T_{s2} values increase with increasing N_k values; however, they decrease with increasing R_r values as noticed and explained already. ii) T_{s1} values increase with decreasing N_k values; as well as increase with decreasing R_r values as noticed and already explained. iii) Eff* values also increases with decreasing N_k values with the increase being more significant at lower values of R_r, especially at R_r values below 1.0. iv) P_{os} values are interesting—as the dynamics are irregular with different N_k values, with P_{os} values sharply increasing initially with decreasing N_k values and at very low R_r values and once after their respective optimal points, P_{os} values again increase but with now increasing N_k values and at high R_r values.

In Figure 4, parameters Q_{s1}, Q_{s2}, P_{os}, T_{s1}, T_{s2} and Eff* are plotted against N_k with $R_r = 0.5 - 2$ and $DT_s = 0.8$ and using $ZT_{i2} = 1$, $N_h = 1$, $T_i = 2.6$—which were fixed throughout the study. $R_r = 0.5 - 2$ instead of only $R_r = 1.7$ was used to see the effects of different R_r values on Q_{s1}, Q_{s2}, P_{os}, T_{s1}, T_{s2} and Eff* at also over different N_k values. As can be seen, Q_{s1}, Q_{s2} and T_{s2} values are directly proportional to N_k. However, T_{s1} and Eff* values are inversely proportional to N_k values. P_{os} initially increases proportionally to N_k till it reaches optimal point at $N_k = 0.25$ in Figure 4c (simple equation) and $N_k = 0.3$ in Figure 4i (simpler equation); after which P_{os} values becomes inversely proportional to N_k. Further noticeable, Q_{s1}, Q_{s2} and T_{s2} values are inversely proportional to R_r values, though directly proportional to N_k values as indicated earlier. Nevertheless, T_{s1} is directly proportional to R_r values but indirectly proportional to N_k. Initially, with increasing N_k, P_{os} increases more with less R_r at mostly low N_k values till maximum P_{os} is attained and thereafter, P_{os} decreases more with less R_r at high N_k values. The optimal P_{os} of 0.0478788 using our simple equation occurs at $R_r = 1.1$ with $N_k = 0.2$, whereas at $R_r = 1.7$, the optimal $P_{os} = 0.0474483$ with $N_k = 0.25$—slightly contrary to [7] which

reported an optimal P_{os} of 0.045 at R_r = 1.7 with N_k = 0.3—which we also have exactly the same result of P_{os} = 0.0451302 at R_r = 1.7 with N_k = 0.3; however, this result was not the exact optimal outcome in our case. Using our simpler equation, we have at R_r = 0.5, two P_{os} optimal values of 0.0966733 and 0.0977376 at respectively N_k = 0.2 and N_k = 0.25. Initially *Eff** with increasing N_k, decreases more with more R_r at mostly low N_k values till optimal *Eff** is attained and thereafter, *Eff** decreases more with less R_r at high N_k values. This *Eff** dynamics is mostly and clearly noticeable in Figure 4l using our simpler equation.

Figure 5 is a 3D plot of Q_{s1}, Q_{s2}, P_{os}, T_{s1}, T_{s2} and *Eff** parameters against R_r = 0.2 − 3.2 but with now DT_s = 0 − 1 and N_k fixed at 0.3. The results summarily reveal that P_{os} and *Eff** increase proportionally with increasing DT_s, reach maximum and decrease, especially at lower R_r values but at higher R_r, P_{os} and *Eff** increase linearly with DT_s. Also, Q_{s1}, Q_{s2}, T_{s1} and T_s parameters exhibit comparable dynamics to those of Figures 3 and 4 results.

Figure 6 is another 3D plot of Q_{s1}, Q_{s2}, P_{os}, T_{s1}, T_{s2} and *Eff** parameters against N_k = 0.05 − 0.5 but now with DT_s = 0 − 1 and R_r fixed at 1.7. As apparent, Q_{s1}, Q_{s2} and T_{s2} have similar dynamics as already noted and discussed earlier in the previous figures. The only difference now is, these dynamics happen across different values of DT_s. The same dynamics applies to T_{s1} and *Eff**. P_{os} generally increases proportionally to DT_s at especially lower N_k values but at higher N_k values, P_{os} decreases with DT_s as revealed.

It's worth stating that, these different plots simply show the different dynamics involved and generally, it's up to designers to now choose optimal values depending on the design constraints and design objectives.

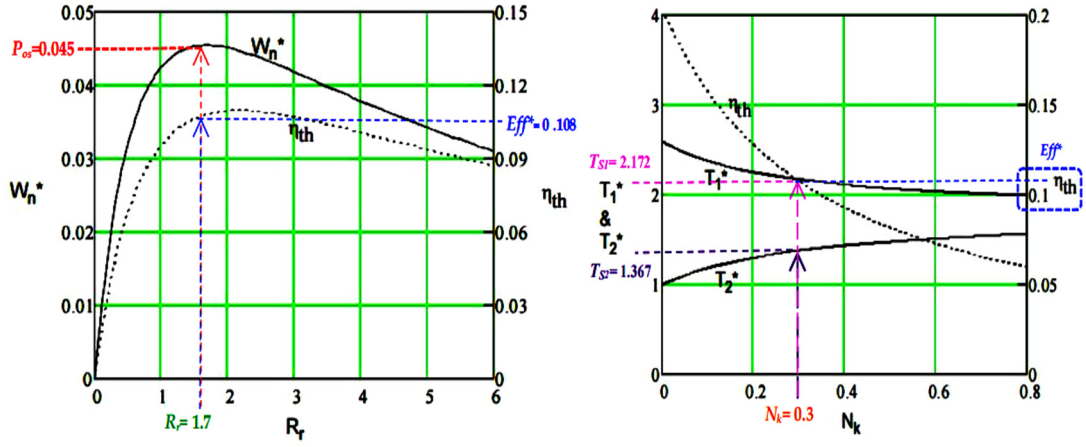

(a) (b)

Figure 7. Figures 2–6 results validator adapted from [7] (Lee H, 2013) (a) P_{os} *(*W_n**) &* *Eff* *(n_{th}) vs R_r; (b) T_1* & T_2* & n_{th} vs N_k.

To validate our findings in Figures 2–6 and Tables 1 and 2 where applicable, Figure 7 and Table 3 results adapted from [7] were used. In summary, validating our findings using [7] results affirms i) exactly the accuracy of our simple equations results and ii) fairly the approximation of our simpler equations results. It should be noted that, just reference [7] was used to validate our findings because a) reference [7] is the original research now developed and simplified with direct analytical formulas

to easily calculate T_{s1} and T_{s2} and therefore it's only prudent to validate the new developments with the original study and b) reference [7] is the only study we know with the aforementioned method and having the stated datasets that we can use.

Table 3. TEG input and output dimensionless and actual results adapted from [7] (Lee H, 2013) to validate Tables 1 and 2.

Inputs	Dimensionless ($W^*_{n,opt}$)	Actual ($W_{n,opt}$)
$T_{\infty\,1}$ = 500 ℃, $T_{\infty\,2}$ = 25 ℃, $\Delta T_{\infty\,1}$ = 475 ℃	N_k = 0.3	n = 254
A = 2 mm^2, L = 1 mm	N_h = 1	$\eta_1 h_1 A_1$ = 4.8 W/K
η_2 = 0.8, h_2 = 60 W/m^{2}K, A_2 = 1000 cm^2	R_r = 1.7	R_L = 1.7 x n x R = 4.32 Ω
$\eta_2 h_2 A_2$ = 4.8 W/K	T^*_∞ = 2.6	$T_{\infty\,1}$ = 500 ℃
Base area A_b of module = 5 cm x 5 cm	$ZT_{\infty\,2}$ = 1.0	ZT_{∞} 2 = 1.0
$\alpha_p = -\alpha_n$ = 220 μV/K	T^*_1 = 2.172	T_1 = 374 ℃
$\mathcal{P}_p = \mathcal{P}_n$ = 1.0 x 10^{-3} Ωcm	T^*_2 = 1.367	T_2 = 137 ℃
$k_p = k_n$ = 1.4 x 10^{-2} W/cmK	W^*_n = 0.045	W_n = 65 W
(Z = 3.457 x 10^{-3} K^{-1})	η_{th} = 0.108	η_{th} = 0.108
(R = 0.01 Ω per thermocouple)	N_I = 0.306	I = 3.9 A
(η_1 = 0.8, h_1 = 60 W/m^{2}K, A_1 = 1000 cm^2)	N_v = 0.5	V = 16.7 V
(Power Density P_d = W_n/A_b W/cm^2)	—	P_d = 2.6 W/cm^2

Compare values with values in Figure 2/Table 2

Check colour coding with the markings on Figure 7

Compare values with values in Figure 2/Table 2

5. Conclusions

Sustainable energy is transcending to become the future of energy to complement the national grid and for private use. As a result, we've researched thermoelectricity (TEG) as an alternative energy source for household applications requiring low DC power and lighting. However, practical TEG use requires heatsinks to work efficiently and reliably but regrettably adding heatsinks add thermal resistances, which consequently degrades the TEG efficiency as well as its output power. We investigated various techniques, especially dimensional analysis and shortlisted the approach by [7]—which converts thermal resistance to convection conductance, making it easier for practical use. However, the formulations in [7] could not find the exact analytical formulas to directly calculate T_{s1} and T_{s2}; as a result, [7] used numerical analysis (a bit cumbersome) which we developed further by introducing DT_s to simplify and derive new simple accurate analytical formulas that can be applied to compute T_{s1} and T_{s2} directly. Furthermore, these simple formulas were further simplified to obtain simpler analytical equations for T_{s1} and T_{s2}. Finally, our simplest T_{s1} and T_{s2} formulas and their optimal relationships were established. These formulas were all verified with chosen optimal values and all gave approximate results that correlated each other. We further used these newly introduced formulas to model, numerically simulate and plotted various characteristics curves of Q_{s1}, Q_{s2}, P_{os}, T_{s1}, T_{s2} and Eff^* against R_r vs N_k vs DT_s using Matlab and Simulink. These results were articulated variously in both 2D and 3D plots and finally the equivalent outcomes were comparatively discussed and validated using each other and as well with results asserted in [7]. In [7], P_{os} of 0.045 is optimal with N_k = 0.3 at R_r = 1.7, contrary to our study which gave optimal P_{os} of 0.0474483 at N_k = 0.25 using our simple equations; however, using our simpler equations, it gave optimal P_{os} of 0.0716775 at N_k = 0.3. Notwithstanding, our simple equations gave P_{os} of 0.0451302 at N_k = 0.3 (though not optimal in our case) which corresponds exactly to optimal P_{os} value of 0.045 with N_k = 0.3 as in [7]. In addition, the magnitude of P_{os} and Eff^* are more (almost doubled) using our simpler Eqs 36 and 37, compared to using our simple Eqs 32 and 33. Furthermore, the optimal values

of P_{os} and *Eff** using both our "simple" and "simpler" equations, respectively occurred at different values of R_r. In sum, *Eff** is best at very low N_k values. The highlights of our study are marked in the various figures and also summarised in Tables 1 and 2. It's worth mentioning that, $DT_s = 0.8$ for this set of optimal values, is rightly only equal to $T_{s1} - T_{s2} = \sim 0.8$ only at $R_r = 1.7$ and $N_k = 0.3$ as summarised in Table 1 and not at any other values when used in both our simple and simpler equations. Finally, in as much as our newly introduced simpler analytical formulas didn't give exact P_{os} and *Eff** results correlating those in i) [7] and ii) our newly introduced analytical simple equations (that gave accurate results), we reckon the simpler equations can be used as first approximation to quickly find T_{s1} and T_{s2} as well as Q_{s1} and Q_{s2} values with fair accuracy. In sum, T_{s1} and T_{s2} are the most vital physical parameters, as they're those that can be easily practically manipulated to achieve the other values. However, first ascertaining the electrical load or R_r value to ensure maximum power transfer is most paramount to achieve optimal result, as a TEG as well TEC, are non-linear devices whose dynamics must be well understood before embarking on a practical design. The next phase of our research is to validate and refine our study practically and then design a household TEG alternative DC power source.

Acknowledgments

Thanks to the Cape Peninsula University of Technology (CPUT) and HySA Systems at the University of the Western Cape (UWC), Cape Town, South Africa for funding the study.

Conflicts of interest

The authors declare no conflict of interest.

Supplementary

Figures 1–6 are provided in link below in picture format for better quality viewing/review.
https://drive.google.com/drive/folders/1VHN2mHJ_wtYaztunL_Sn21XJmppc0o8z?usp=sharing

References

1. Van der Walt ML, Van den Berg J, Cameron M (2017) South Africa department of energy, state of renewable energy in South Africa. Available from: http://www.energy.gov.za/files/media/Pub/2017-State-of-Renewable-Energy-in-South-Africa.pdf.
2. Bayendang NP, Kahn MT, Balyan V, et al. (2020) A comprehensive thermoelectric generator (TEG) Modelling. *AIUE Congress 2020: Energy and Human Habitat Conference*, Cape Town, South Africa, 2020; Zenodo: Geneva, Switzerland, 2020: 1–7. Available from: http://doi.org/10.5281/zenodo.4289574.
3. Bayendang NP, Kahn MT, Balyan V, et al. (2020) A comprehensive thermoelectric cooler (TEC) modelling. *AIUE Congress 2020: International Conference on Use of Energy*, Cape Town, South Africa; SSRN: Rochester, NY, USA, 2021: 1–7. Available from: https://ssrn.com/abstract=3735378 or http://dx.doi.org/10.2139/ssrn.3735378.

4. Twaha S, Zhu J, Yan Y, et al. (2016) A comprehensive review of thermoelectric technology: materials, applications, modelling and performance improvement. *Renewable Sustainable Energy Rev* 65: 698–726.
5. Jouhara H, Żabnieńska-Góra A, Khordehgah N, et al. (2021) Thermoelectric Generator (TEG) technologies and applications. *Int J Thermofluids* 9: 100063.
6. Bayendang NP, Kahn MT, Balyan V (2021) Simplified thermoelectric cooler (TEC) with heatsinks modeling and simulation using Matlab and Simulink based-on dimensional analysis. *AIUE Conference 2021: 2nd Energy and Human Habitat Conference*, Cape Town, South Africa; SSRN: Rochester, NY, USA, 1–8. Available from: http://dx.doi.org/10.2139/ssrn.3900757.
7. Lee H (2013) Optimal design of thermoelectric devices with dimensional analysis. *Appl Energy* 106: 79–88.
8. Lineykin S, Ruchaevski I, Kuperman A (2014) Analysis and optimization of TEG-heatsink waste energy harvesting system for low temperature gradients. *16th European conference on power electronics and applications*, Lappeenranta, Finland, 1–10.
9. Melnikov AA, Kostishin VG, Alenkov VV (2017) Dimensionless model of a thermoelectric cooling device operating at real heat transfer conditions maximum cooling capacity mode. *J Electron Mater* 46: 2737–2745.
10. Li W, Paul MC, Montecucco A, et al. (2015) Multiphysics simulations of a thermoelectric generator. *The 7th international conference on applied energy—ICAE 2015*, *Energy Proc* 75: 633–638.
11. Casano G, Piva S (2012) Parametric thermal analysis of the performance of a thermoelectric generator. *6th European thermal sciences conference (Eurotherm 2012)*, Poitiers, France, *J Physics*: *Conference Series*, 395: 2156.
12. Dos Santos Guzella M, Dos Santos GR, Cabezas-Gómez L, et al. (2021) Numerical simulation of the two-dimensional heat diffusion in the cold substrate and performance analysis of a thermoelectric air cooler using the lattice Boltzmann method. *Int J Appl Comput Math 7*: 130.
13. Hao J, Qiu H, Ren J, et al. (2020) Multi-parameters analysis and optimization of a typical thermoelectric cooler based on the dimensional analysis and experimental validation. *Energy* 205: 118043.
14. Lu X, Zhao D, Ma T, et al. (2018) Thermal resistance matching for thermoelectric cooling systems. *Energy Convers Manage* 169: 186–193.
15. Chen J, Lin B, Wang H, et al. (2000) Optimal design of a multi-couple thermoelectric generator. *Semicond, Sci Technol* 15: 184–188.
16. Lineykin S, Ben-Yaakov S (2006) A Simple and intuitive graphical approach to the design of thermoelectric cooling systems. *37th IEEE Power Electronics Specialists Conference*, Jeju, Korea (South), 1–5.
17. Hubbard WA, Mecklenburg M, Lodico JJ, et al. (2020) Electron-transparent thermoelectric coolers demonstrated with nano-particle and condensation thermometry. *ACS Nano* 14: 11510–11517.
18. He W, Wang S, Yang Y (2016) Optimal heat exchanger dimensional analysis under different automobile exhaust temperatures for thermoelectric generator system. *Energy Proc* 104: 366–371.